Circular Economy 2 (2023) 100063

Contents lists available at ScienceDirect

Circular Economy

journal homepage: www.journals.elsevier.com/circular-economy

Review

Recent advances of research in coal and biomass co-firing for electricity and heat generation

Li Liu [a], Muhammad Zaki Memon [b], Yuanbo Xie [c], Shitie Gao [d], You Guo [e], Jingliang Dong [f], Yuan Gao [a], Aimin Li [a], Guozhao Ji [a, *]

[a] Key Laboratory of Industrial Ecology and Environmental Engineering, School of Environmental Science & Technology, Dalian University of Technology, Dalian 116024, China
[b] Department of Energy Systems Engineering, Quaid-e-Awam University of Engineering, Science and Technology, Nawabshah 67480, Pakistan
[c] Tianyun Low-carbon New Energy Technology Co Ltd, Dalian 116033, China
[d] Shenyang Yunyuan Robot Technology Co., Ltd., Shenyang 110065, China
[e] Fushun Supervision & Inspection Institute for Special Equipment, Fushun 113009, China
[f] Institute for Sustainable Industries & Liveable Cities, Victoria University, PO Box 14428, Melbourne, VIC 3011, Australia

ARTICLE INFO

Article history:
Received 19 April 2023
Received in revised form
26 September 2023
Accepted 24 October 2023
Available online 23 November 2023

Keywords:
Coal
Biomass
Co-firing
Synergistic effect
Antagonistic effect

ABSTRACT

Coal-fired power generation resulted in a shortage of conventional fossil fuels and an increase in greenhouse gas emissions. The co-firing of coal and biomass waste in coal-fired boilers was a promising strategy to supplement the energy source and reduce greenhouse gases. However, the co-firing mechanism and potential problems were not well understood. Therefore, the differences between coal and biomass in properties such as proximate and ultimate composition, components in ash and the calorific value were first discussed. Next, compared with the combustion of coal alone, this review analyzed the discrepancies and corresponding issues of co-firing in combustion behaviors and products such as ash and gaseous pollutants. Finally, this review outlined how operational conditions could affect the co-firing performance.

1. Introduction

With the continuous development of social economy and the continuous emission of CO_2, the global warming caused by the greenhouse effect is threatening the eco-system. Therefore, in response to global climate change, the Paris Agreement was adopted at the Paris Climate Conference in 2016 (United Nations, 2016). To achieve the targets of the Paris Agreement, China pledged to make efforts to reach the pinnacle of carbon emissions by 2030 and attain carbon neutrality by 2060 at the 75th United Nations General Assembly on September 22, 2020 (Zhang et al., 2021). Although the proportion of coal consumption in total energy consumption decreased from 62.2% in 2016 to 56.8% in 2020 (see Fig. 1), it can be seen that coal is still the main energy consumption resource in China (National Bureau of Statistics, 2021). According to the Annual Development Report of Power Industry for China 2021, at the end of 2020, the total installed capacity of power generation in China was 220.204 million kilowatt hours, and the installed capacity of coal power generation was 107.912 million kilowatt hours, accounting for 49% of the total installed capacity of power generation. The result showed that coal was also the largest energy consumption resource in power industry (China Electricity Council, 2021). At a global level, due to the development of clean energy resource in power industry, the share of coal-fired power generation had already decreased by 3% and 4.6% in 2019 and 2020, respectively. However, the share of global coal-fired power generation stared to increase in 2021, resulting from raising gas prices in the United States and Europe and increased economic activity in China (IEA, 2021). In summary, the power industry urgently needs to seek for clean energy resources to partially replace coal in order to alleviate the problems caused by the large amount of CO_2 emissions resulting from coal combustion.

Biomass is regarded as an alternative clean energy resource. The utilization of biomass to partially replace coal for power generation can not only reduce CO_2 emissions, but also even achieve negative CO_2 emissions by combining carbon capture technology (Liu et al.,

* Corresponding author.
E-mail address: guozhaoji@dlut.edu.cn (G. Ji).

https://doi.org/10.1016/j.cec.2023.100063

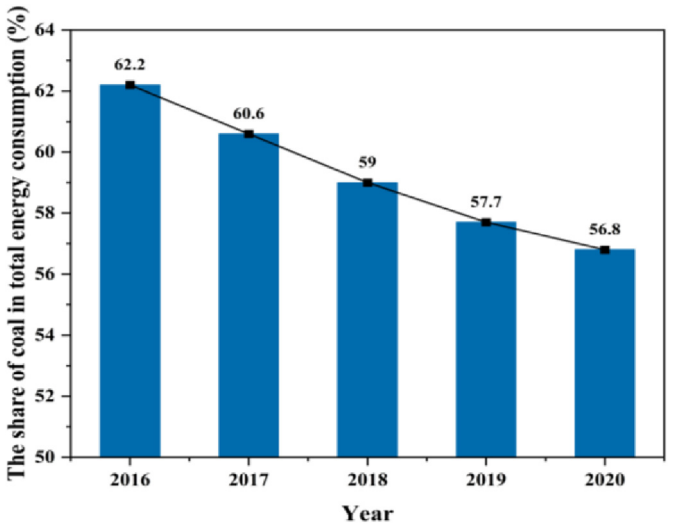

Fig. 1. The share of coal in total energy consumption for the period 2016 to 2020 in China (China Electricity Council, 2021).

2022b; Spiegl et al., 2021). Many studies also found that co-firing of coal and biomass was conducive to reducing the emissions of other pollutants such as CO, NO_x, SO_2 and $PM_{2.5}$ (Gungor, 2013; Jiang et al., 2022; Zhang et al., 2020). Besides the theoretical validation of numerical simulations and experimental research, the fact that the co-firing of coal and biomass causes reduction of partial pollutant emissions was proved by practice. In 2018, the Notice on the Construction of Pilot Projects for Coal Fired Biomass Power Generation Technology Transformation jointly issued by the National Energy Administration and the Ministry of Ecology and Environment announced 84 pilot projects. The main technologies used in these projects were the direct co-firing of coal and dried sludge, and the indirect co-firing of coal with gasification products from biomass waste from forestry and agriculture. A 72-h trial run for a 640 MW supercritical coal-fired plant was successfully accomplished. According to the estimates, the project would reduce coal consumption of roughly 20,000 tons annually, and result in a reduction of 159, 175 and 40,000 tons per year in SO_x, NO_x and CO_2 emissions, respectively. Obviously, the project significantly reduced gaseous pollutant emissions (National Energy Administration, 2018).

With continuous consumption of coal, the global coal reservoirs are declining. Biomass energy can lighten the energy crisis caused by the consumption of non-renewable energy (Saleem, 2022). Apart from a few countries with high levels of hydropower such as Norway, Canada, New Zealand and Switzerland, biomass power generation is the mainstream alternative in most countries (IEA Bioenergy, 2022). For example, China is also rich in biomass energy storage. From 2010 to 2019, the total biomass energy from terrestrial ecosystems was estimated to be 535.91×10^{18} J, equivalent to 18.29 Gt standard coal. The total biomass from forest ecosystems was the most abundant, which has the greatest potential to partially replace coal (Yan et al., 2020) (see Table 1). Facing the huge biological energy resources, it is imperative to utilize biomass waste to meet the energy demand and alleviate environmental pollution caused by coal combustion for power generation.

Table 1
Biomass energy and standard coal equivalent in different terrestrial ecosystems in China from 2010 to 2019 (Yan et al., 2020).

Type of terrestrial ecosystem	Biomass energy (EJ)	Standard coal (Gt)
Forest	434.83	14.84
Grassland	87.48	2.98
Cropland	13.6	0.46

Currently, most power generation devices are designed for coal combustion, and it is rare to find boiler designed for biomass alone. To fully utilize the existing coal power generation devices with the least retrofitting, co-firing of coal with biomass waste is the most feasible option. In addition, compared with pure biomass combustion power generation, co-firing technology of coal and biomass has higher power generation efficiency, lower equipment and operating costs, high flexibility of different biomass (Xu et al., 2020). Despite the fact that co-firing of coal and biomass has several benefits, adding biomass to coal-fired boilers will inevitably result in a number of different phenomena from combustion of coal alone, because the existing coal-fired boilers are specifically designed for coal combustion. Numerous studies about experiments and numerical simulations have been conducted to investigate co-firing (see Table 2). Although some of the above studies have proved the feasibility of co-firing of coal with biomass at the laboratory experimental level, the phenomena of co-firing tend to be more complex in industrial boilers than in small experimental reactors. For example, with the increase of biomass loading, the temperature tends to decrease with the height of the whole furnace for experimental reactors. However, in a 260 t/h circulating fluidized bed (CFB) industrial boiler, with the increase of biomass mixing ratio, when the height increase the temperature increased at the upper part of the furnace due to more volatiles in biomass, while the temperature decrease at the bottom of furnace due to lower calorific value of coal and biomass mixture (Liu et al., 2012).

Additionally, it is critical to comprehend the potential issues that could result from the co-firing of biomass in coal-fired boilers. The risks of unit shutdown caused by the co-firing of coal and biomass can be avoided or reduced with the increased understanding of the co-firing process. Knowledge of biomass properties will facilitate understanding of complex co-firing challenge in existing coal-fired boilers. Biomass is graded as a very low-rank fuel. Compared to coal, biomass has high moisture, ash, O-content and low calorific value. Properties of biomass vary significantly due to the wide range of biomass types, which lead to different retrofitting of equipment and adjustment of operating conditions when switching to different biomass in co-firing with coal. During the co-firing of coal and soybean straw, which has high ash content, CO_2 emission was reduced by increasing the amount of biomass. However, as the ratio of biomass in the mixture increases, the increased ash content began to melt and stick to the equipment. To reduce the adhesion of ash to equipment, it is necessary to spray smooth material to equipment and seek the appropriate operating conditions such as suitable blending ratio of biomass (Yao et al., 2020a). Priyanto et al. (2017) reported that the co-firing of coal and wood in a 150-MW class pulverized-coal boiler was more likely to cause the corrosion of the boiler heat-transfer tubes inside furnace wall than the combustion of pure coal. Measurements for compounds contents of the deposits in the tubes revealed that the co-firing generated two to three times more potassium sulfate and sodium sulfate than combustion of coal, which was likely to be the reason of the corrosion in the tubes. Moreover, the co-firing yielded more unburned carbon in furnace wall, which demonstrated the presence of a strong reducing atmosphere. The results indicated that the boiler heat-transfer tubes required anti-corrosion coatings to reduce corrosion and the furnace demanded to increase air flow for reduction of unburned carbon.

The aim of this review is to minimize the negative effects of co-firing of biomass with coal in coal-fired boilers. Firstly, the distinctions between coal and biomass are described. Next, the differences between pure coal combustion and the co-firing of coal

Table 2
The different phenomena between co-firing of coal and biomass and combustion of coal in experiments and numerical simulations.

Method	Theme	Phenomena	Refs
Experiment	Ash slag characteristics	The ash particles formed from co-firing coal with each of the two types of biomass are more prone to agglomerate and slag compared to the ash particles formed from burning coal alone.	Mu et al. (2022)
Experiment	Co-firing characteristics	Compared to burning coal alone, the ignition temperature and burnout temperature are lower when coal co-fired with two types of biomass, separately.	Liu et al., (2022b); Sakthivel et al. (2018)
Experiment	NO_x emission	Compared to burning pure bituminous coal, adding spent coffee grounds for co-firing with bituminous coal reduce NO_x emissions.	Garcia et al. (2022)
Experiment	SO_2 emission	When lignite or bituminous coal are co-fired with cedarnut shell, compared to burning coal alone, co-firing cedarnut shell with lignite does not reduce SO_2 emissions. However, co-firing cedarnut shell with bituminous coal reduces SO_2 emissions.	Jerzak et al. (2018)
Numerical simulation	CO_2 emission	Compared to burning coal alone, adding 20% biomass for co-firing with coal can reduce CO_2 emissions.	Mikulcic et al. (2019)
Numerical simulation	NO emission	As the mass ratio of biomass increases, the NO from the co-firing of coal and biomass keeps decreasing.	Yang et al. (2021b); Zhou et al., (2020a)
Numerical simulation	NO and SO_2 emission	As the mass ratio of dried sawmill sludge increases, the NO and SO_2 produced by co-firing Longyan anthracite and dried sawmill sludge also increase.	Zhang and Zeng (2019)
Numerical simulation	NO emission co-firing	Compared with pure coal combustion, the co-firing of wheat, corn or cotton straw with coal produces less NO, with wheat straw co-firing with coal producing the least NO.	Li et al. (2020)

and biomass are considered. The potential issues arising from co-firing are also presented. Finally, some solutions such as torrefaction for the above issues are offered.

2. Comparison of coals and biomasses

According to the classification standard of coal, coal can be divided into lignite, bituminous coal and anthracite by the content of parameters of coalification degree such as volatile matter based on dry ash-free basis (daf). The volatile matter (for example, daf) of lignite is the highest and that of anthracite is the lowest (Standardization Administration, 2009). There are many different types of biomass, and up until now there has not been a standard classification for biomass. Biomass can be categorized into the following groups based on its characteristics (Jenkins et al., 1998): ligneous biomass (herbs and other annual plants (straw, grass, leaves, etc.)); agricultural by-products and waste (shells, kernels, etc.); refuse derived fuel; and other wastes (municipal sludge, etc.). The primary components of coal and biomass are fixed carbon, volatile matter, water, and ash. The primary elements of coal and biomass are C, H, O, N, and S. The calorific value of coal and biomass depends on the content of C, H, and O. Compared to coal, biomass has a lower calorific value because it contains more oxygen and less carbon (Given et al., 1986). The fundamental reason is that C—O bonds have lower energy than C—C bonds. The presence of N and S in coal and biomass has been linked to the formation of NO_x and SO_x (Munir et al., 2009; Tao et al., 2012). The amount of slagging and fouling in the furnace is influenced by the ash content, which has an impact on combustion efficiency and operation stability (Li et al., 2021). As a result, it is critical to conduct the ultimate, proximate, and ash analysis to study co-firing phenomena in accordance with the aforementioned classification of coal and biomass. This information is essential for determining any potential issues resulting from the co-firing of coal and biomass, as well as for assisting power plants to select proper coal and biomass.

Table 3 shows that the proportion of fixed carbon in some coal is high, up to 70%. An evident difference between coal and biomass from the proximate analysis is that coal has much higher fraction of fixed carbon, which leads to longer combustion time when firing coal compared with firing biomass. Generally, the content of fixed carbon in all types of coal is above 30%, and that of the fixed carbon in all types of biomasses is below 20%. It can be observed from the ultimate analysis that a distinct feature of biomass is the high O content. For example, the O fraction is up to 68.13% in waste wood. In general, the content of N and S in coal is much higher than that in biomass. The main ash component in coal and biomass is SiO_2. In addition, the main ash components of biomass are CaO and K_2O, while the main ash component of coal is Al_2O_3. These various components in ash can affect the extent of slagging. However, these effects are extremely complex and vary depending on conditions such as temperature, pressure, and oxygen concentration. Therefore, it is necessary to conduct specific experiments to determine how different ash components affect slagging. Apart from elements and components, the higher heating values of fuels are also significantly important for firing, which indicated the amount of heat released after coal and biomass are completely combusted. It is noteworthy that the higher heating values include the released heat of water vapor condensation. In Fig. 2, the higher heating values of coals are higher than that of biomasses, which demonstrates coals provide more heat than biomasses. Thus, coal is more superior to biomass as a fuel.

In addition, the proximate, ultimate and ash analysis of different biomass are quite different. The main composition of most biomass is volatile matter, with a content of about 70%. However, a few exceptions such as sludge and waste wood showed lower volatile matter (~40%) due to the richness of ash (~40%). The main elements of different biomass are C and O, with relatively low contents of N and S. However, the proportion of N and S in different biomass can differ by several orders of magnitude. For example, the N content in walnut wood is about 4%, while that in poplar wood is about 0.3%. While durian shell only contains 0.01% of S, printing and dyeing textile sludge contains roughly 3% of S. The content of CaO and K_2O in the ash of the most ligneous biomass is the highest. The content of SiO_2 and K_2O in the ash of the most herbaceous biomass is the richest. SiO_2 is the main ash component of rice husk which accounts for 80%—90%. The ash compounds of garbage derived and

Table 3
Approximate, ultimate and ash analysis of coals and biomasses (M = moisture; A = ash; V = volatile matter; FC = fixed carbon).

Analysis of coals									
Lignite									
Location	Barsingsar, India	Suruka, India	SLPP, India	Kasimkota	Turkey	Wenlan, China	Xiaolongtan, China	Wuchang, Hubei, China	Zhundong, Xinjiang Uygur Autonomous Region, China
Approximate analysis (wt%, ad)									
M	7.9	9.1	14.7	13.5	16.4	1.82	13.90	6.80	16.40
A	24.6	39.9	16.5	9.6	42.0	26.30	15.08	39.25	25.00
V	35.7	29.3	37.3	38.4	33.6	32.89	39.53	25.15	3.24
FC	31.8	21.7	31.5	38.5	8.0	38.99	31.49	28.80	55.36
Ultimate analysis (wt%, ad)									
C	47.40	32.31	49.75	56.50	28.50	60.75	46.56	39.91	65.69
H	3.80	2.63	3.66	3.50	1.50	4.56	3.72	2.98	3.13
O	47.00	58.62	44.76	38.50	65.70	2.96	17.90	10.29	9.81
N	1.30	1.07	0.63	1.20	1.00	1.23	1.38	0.28	1.30
S	0.50	5.37	1.20	0.30	3.30	2.38	1.46	0.49	0.43
Components of ash (wt%)									
SiO_2	43.7	43.5	41.7	45.5	34.2	55.82	21.13	66.74	26.10
Al_2O_3	39.1	28.8	14.4	29.7	13.3	10.28	13.32	16.88	32.70
Fe_2O_3	0.8	2.3	14.0	1.5	5.7	5.97	9.58	4.07	4.59
TiO_2	0.8	2.3	0.9	3.3	0.6	_	_	6.57	0.25
CaO	6.1	3.9	18.4	14.4	22.9	5.50	39.16	1.50	3.05
MgO	2.1	0.7	3.2	4.1	2.9	4.80	2.34	0.72	0.55
Na_2O	2.3	0.4	1.5	0.4	0.5	5.71	0.27	0.56	5.73
K_2O	0.1	0.2	1.0	0.3	0.8	1.12	0.96	4.30	0.49
SO_3	0.2	2.8	4.8	_	17.5	2.42	_	_	16.21
P_2O_5	_	_	_	_	_	_	0.07	_	0.11
Reference	Selvakumaran and Bakthavatsalam (2015)					Zhao et al. (2013)	Zhou et al. (2020b)	Guo et al. (2019)	Wang et al. (2017)
Bituminous coal									
Location	Illinois, USA	Utah, USA	Sufco, Utah, USA	China	China	China	China	Shuozhou, Shanxi, China	Datong, Shanxi, China
Approximate analysis (wt%, ad)									
M	9.65	3.18	6.11	3.54	2.64	6.7	2.5	2.4	6.20
A	7.99	8.83	8.36	30.38	18.45	14.8	9.0	29.5	19.15
V	36.78	38.6	38.49	33.27	30.84	32.2	30.6	24.4	29.26
FC	45.58	49.36	47.04	32.81	48.07	46.3	57.9	43.7	45.39
Ultimate analysis (wt%, ad)									
C	64.67	70.60	67.87	46.81	51.40	64.1	75.4	57.1	59.70
H	5.59	5.41	5.45	3.64	2.80	4.3	4.3	3.83	3.62
O	16.65	13.21	16.87	12.69	7.35	8.2	7.3	4.15	9.91
N	1.12	1.42	1.09	2.72	0.73	0.8	1.3	1.14	1.04
S	3.98	0.53	0.36	0.22	2.29	1.1	0.2	1.88	0.39
Components of ash (wt%)									
SiO_2	49.28	60.89	46.85	57.51	53.32	52.5	50.07	45.81	50.40
Al_2O_3	17.66	14.52	8.34	28.30	29.98	19.4	20.65	40.92	34.60
Fe_2O_3	14.57	5.09	5.25	1.94	5.66	4.2	7.34	0.98	1.56
TiO_2	0.85	0.88	0.64	_	_	_	_	_	1.25
CaO	1.87	6.11	18.21	2.25	5.29	11.9	10.62	0.12	6.31
MgO	0.98	1.39	2.84	2.19	1.04	0.9	1.63	0.06	0.23

Na_2O	1.51	1.41	3.09	4.25	0.47	3.4	2.81	0.47	0.10
K_2O	2.26	0.57	0.33	1.11	0.40	1.9	1.25	0.04	0.44
SO_3	2.22	2.33	5.96	1.60	_	2.4	1.57	4.65	2.40
P_2O_5	0.11	0.59	0.01	0.85	_	3.4	2.57	0.11	_
MnO	0.02	0.02	_	_	_	_	_	_	_
MnO_2	_	_	0.05	_	_	_	_	_	_
Al_2O_2	_	_	_	_	29.98	_	_	_	_
S	_	_	_	_	0.67	_	_	_	_
Cl	_	_	_	_	_	_	1.46	_	_
Reference	Yu et al. (2011)		Liu et al. (2020b)	Xu et al. (2014)	Yin et al. (2012)	Wu et al. (2019)	Li et al. (2022b)	Wang et al. (2015)	Li et al. (2017)
Bituminous coal				Anthracite					
	Wucaiwan, Xinjiang Uygur Autonomous Region, China	Zijin, Xinjiang Uygur Autonomous Region, China	Huangling, Shanxi, China	Korea	Jingcheng, Shanxi, China				
Approximate analysis (wt%, ad)									
M	13.05	14.30	3.80	2.0	2.23	1.83	4.00	2.29	1.17
A	6.30	3.52	11.02	4.7	20.10	22.0	30.24	17.85	17.40
V	26.39	28.42	32.10	3.8	8.46	7.52	6.72	8.11	9.08
FC	54.26	53.76	53.08	89.5	69.21	68.45	59.04	72.00	72.35
Ultimate analysis (wt%, ad)									
C	65.77	64.77	67.97	89.9	65.81	66.95	59.35	71.27	73.31
H	2.77	3.72	4.22	1.1	3.25	2.61	2.56	3.025	2.87
O	10.96	12.34	11.69	7.8	6.72	4.98	1.29	4.95	3.39
N	0.49	0.77	0.83	0.8	0.94	0.80	0.72	0.92	1.07
S	0.66	0.58	0.47	0.4	0.95	1.23	1.84	0.86	0.79
Components of ash (wt%)									
SiO_2	17.08	15.90	38.60	49.2	52.5	54.19	44.23	52.94	47.00
Al_2O_3	6.99	11.67	20.60	35.6	29.0	27.91	36.04	29.31	33.55
Fe_2O_3	11.60	20.33	10.60	0.8	4.44	4.23	5.27	4.03	7.99
TiO_2	0.61	1.56	_	0.5	1.05	0.97	0.25	1.07	0.85
CaO	27.53	15.26	16.00	8.0	5.18	4.87	2.99	4.94	5.16
MgO	7.42	3.04	1.94	2.5	1.12	1.08	0.55	1.67	1.60
Na_2O	6.08	12.77	0.73	2.4	1.25	1.89	5.73	1.19	0.46
K_2O	0.46	0.63	1.94	0.1	1.87	1.84	0.49	1.55	0.38
SO_3	21.65	15.10	7.77	3.1	1.97	2.09	16.21	2.32	2.92
P_2O_5	_	_	_	_	0.254	0.25	0.11	0.78	_
Cl	_	_	0.02	_	_	_	_	0.15	_
Reference	Wang et al. (2019)		Lv et al. (2022)	Selvakumaran and Bakthavatsalam (2015)	Jing et al. (2016)	Lu et al. (2018)	Wang et al. (2017)	Yao et al. (2020b)	Xie et al. (2021)
Analysis of biomasses									
Ligneous materials									
	Candlenut wood	Poplar	Wood of *P. orientalis*	Incense sticks	Waste wood	Pine sawdust			
Approximate analysis (wt%, ad)									
M	9.90	2.42	2.5	7.91	0.52	10.09	7.89	2.06	3.45
A	1.40	0.59	2.1	14.53	44.99	0.71	0.71	0.99	1.98
V	74.23	82.13	83.3	71.86	45.94	76.83	77.67	82.90	76.50

(*continued on next page*)

Table 3 (*continued*)

Analysis of biomasses									
Ligneous materials									
	Candlenut wood	Poplar	Wood of *P. orientalis*	Incense sticks	Waste wood	Pine sawdust			
FC	14.47	14.86	12.1	5.70	8.54	12.37	14.34	14.05	18.07
Ultimate analysis (wt%, ad)									
C	43.64	47.08	45.7	36.54	28.08	49.61	49.55	50.78	52.01
H	5.04	6.38	5.3	4.90	3.42	5.7	6.11	5.83	5.40
O	35.94	43.01	41.3	35.59	68.13	44.47	41.08	39.68	41.97
N	4.04	0.28	0.5	0.40	0.37	0.19	0.25	0.10	0.13
S	0.04	0.04	0.0	0.12	_	0.01	0.33	0.56	0.02
Components of ash (wt%)									
SiO_2	19.23	5.69	4.50	3.04	71.06	12.68	12.83	11.87	11.9
Al_2O_3	4.16	2.14	2.35	0.76	7.95	2.74	3.53	5.90	2.43
Fe_2O_3	6.36	1.58	0.73	2.54	6.69	2.46	2.79	5.08	2.45
TiO_2	_	0.12	_	0.09	0.37	0.24	0.067	_	0.22
CaO	25.28	43.90	57.62	60.80	5.86	35.91	36.86	41.78	36.78
MgO	3.98	3.69	5.61	22.25	1.20	12.66	6.05	7.35	12.98
Na_2O	1.41	2.67	1.98	2.10	1.01	2.93	3.04	_	3.04
K_2O	17.09	33.74	12.16	_	1.99	21.39	11.12	3.91	22.65
SO_3	0.51	6.47	5.81	1.57	0.76	3.24	12.08	5.47	2.89
P_2O_5	1.84	_	8.28	0.40	1.79	5.09	7.41	1.32	4.19
Cl	0.138	_	0.88	0.726	_	0.24	1.53	_	0.2
Cl_2O	_	_	_	_	0.57	_	_	_	_
Cr_2O_3	_	_	_	_	0.53	_	_	_	_
MnO	_	_	_	_	0.14	_	_	_	_
CuO	_	_	_	_	0.03	_	_	_	_
ZnO	_	_	_	_	0.04	_	_	_	_
Reference	Deng et al. (2013)	Wang et al. (2021b)	Li et al. (2022b)	Wen et al. (2021)	Yang et al. (2022)	Jing et al. (2016)	Yao et al. (2020b)	Liu et al. (2021)	Lu et al. (2018)
Herbs and other annual plants									
Rice straw							Wheat straw		
Approximate analysis (wt%, ad)									
M	2.89	8.38	7.00	1.51	6.55	6.82	7.70	9.89	7.66
A	14.61	12.53	14.18	11.31	8.54	11.39	6.28	5.22	9.93
V	64.8	64.74	70.58	69.09	73.49	68.17	69.49	68.39	74.4
FC	17.7	14.35	8.24	18.09	11.42	13.62	16.53	16.50	15.67
Ultimate analysis (wt%, ad)									
C	49.13	38.54	37.63	42.66	41.02	39.48	40.71	45.55	37.52
H	5.54	4.15	5.47	5.68	3.83	4.94	4.59	5.70	4.33
O	26.13	35.56	34.79	37.37	38.06	36.22	40.31	46.53	39.68
N	1.27	0.65	0.77	1.03	1.72	1.05	0.18	1.32	0.64
S	0.43	0.19	0.16	0.44	0.28	0.10	0.23	0.15	0.23
Components of ash (wt%)									
SiO_2	58.81	66.47	36.45	38.60	43.71	43.58	38.44	30.09	31.30

Al_2O_3	0.34	_	3.02	1.69	1.96	4.11	1.32	1.67	1.30
Fe_2O_3	0.52	_	0.59	_	0.58	0.34	0.93	1.01	0.60
TiO_2	_	_	_	_	_	_	_	0.15	_
CaO	3.89	2.69	8.48	5.56	7.89	2.54	7.99	4.80	10.10
MgO	2.74	1.15	_	5.12	6.90	2.13	2.71	5.09	3.95
Na_2O	0.74	0.60	_	0.996	3.47	2.93	0.83	13.24	0.35
K_2O	20.45	17.21	30.54	15.53	19.53	29.44	27.86	32.60	34.30
SO_3	3.09	2.59	1.611	2.93	4.18	_	8.51	3.45	8.31
P_2O_5	2.08	0.68	0.27	3.20	2.75	1.58	1.46	7.72	_
Cl	5.63	0.612	_	_	6.73	_	0.783	1.97	4.54
MnO	_	_	1.08	_	1.80	_	_	_	_

Reference	Wang et al. (2020)	Deng et al. (2013)	Mostafa et al. (2021)	Liu et al. (2021)	Liu et al. (2022b)	Jun et al. (2020)	Deng et al. (2013)	Jing et al. (2016)	Lv et al. (2022)
Cotton stalk							Green leaf	Yellow leaf	Water hyacinth
Approximate analysis (wt%, ad)									
M	2.24	2.46	9.19	9.75	3.41	10.08	3.9	5.5	9.95
A	3.62	3.38	3.51	6.40	5.44	7.45	8.0	8.1	17.4
V	72.82	74.65	69.56	67.59	76.47	65.38	75.1	73.3	56.30
FC	21.32	19.51	17.74	16.26	14.68	17.09	13.0	13.1	16.35
Ultimate analysis (wt%, ad)									
C	47.50	47.69	43.10	41.68	44.67	43.51	46.7	46.7	36.62
H	5.92	5.96	4.62	4.41	5.99	5.69	6.0	5.8	5.28
O	44.89	45.23	38.43	36.55	38.18	31.42	33.4	33.1	27.49
N	0.64	0.49	0.96	0.98	0.45	1.54	1.8	0.6	3.01
S	0.79	0.63	0.19	0.23	0.168	0.31	0.3	0.2	0.25
Components of ash (wt%)									
SiO_2	11.99	11.09	3.60	35.92	38.06	53.37	18.97	21.53	0.41
Al_2O_3	8.03	8.24	1.11	2.81	6.63	2.94	_	0.65	0.18
Fe_2O_3	0.88	0.85	_	_	3.00	1.46	1.73	1.17	0.10
TiO_2	_	_	0.12	0.12	0.30	0.16	_	_	0.01
CaO	22.54	22.15	18.75	6.89	10.36	7.17	46.87	50.62	0.23
MgO	6.98	7.02	7.52	4.38	8.33	4.06	0.6	4.51	_
Na_2O	3.62	3.59	2.92	0.58	1.43	0.86	_	_	0.18
K_2O	24.90	29.17	31.08	30.44	13.55	1.61	13.67	5.87	14.11
SO_3	4.12	3.96	6.32	5.04	6.95	1.49	11.1	6.58	_
P_2O_5	6.82	5.91	2.01	0.82	1.17	_	6.36	2.46	0.35
Cl	_	_	0.558	0.540	_	3.10	0.12	0.13	_

(*continued on next page*)

Table 3 (*continued*)

Cotton stalk							Green leaf	Yellow leaf	Water hyacinth
Cl_2O	5.87	4.79	_	_	_	_	_	_	_
MnO	_	_	_	_	_	_	_	_	0.05
Reference	Li et al. (2019)	Li et al. (2022b)	Deng et al. (2013)	Deng et al. (2013)	Lu et al. (2018)	Xie et al. (2021)	Li et al. (2022b)	Li et al. (2022b)	Huang et al. (2018)
Agricultural by-products and wastes								Refuse derived fuel and other wastes	
Refuse derived fuel and other waste					Peanut shell	Durian shell	Waste tea	Textile dyeing sludge	Sewage sludge
Approximate analysis (wt%, ad)									
M	9.30	7.45	8.16	10.4	6.75	2.95	5.45	7.09	7.57
A	12.91	11.67	33.67	15.1	7.48	5.67	82.31	43.69	46.63
V	63.19	73.08	48.94	60.8	66.72	72.56	6.15	47.84	40.22
FC	14.60	7.08	9.46	13.8	19.05	18.82	6.09	1.38	5.58
Ultimate analysis (wt%, ad)									
C	38.25	39.88	28.47	35.8	43.76	43.91	47.99	21.06	24.13
H	1.69	5.54	4.15	5.1	4.80	5.87	6.60	4.35	3.94
O	37.46	36.71	24.42	33.1	36.09	40.03	28.73	18.51	12.49
N	0.34	0.46	1.05	0.4	1.00	1.47	4.90	2.46	4.50
S	0.05	0.48	0.10	0.1	0.12	0.01	0.18	2.84	0.74
Components of ash (wt%)									
SiO_2	90.09	87.27	88.51	89.9	58.42	2.37	2.14	7.18	2.81
Al_2O_3	_	0.74	1.73	_	9.23	0.48	4.23	57.62	1.59
Fe_2O_3	0.54	0.77	1.10	0.4	3.26	0.41	1.18	17.13	14.28
TiO_2	_	0.05	0.18	_	0.64	_	_	_	0.20
CaO	0.84	2.38	1.31	1.7	8.93	4.49	36.55	4.21	11.20
MgO	_	0.73	0.84	_	2.71	12.05	8.63	0.42	0.25
Na_2O	0.01	0.14	0.31	_	1.80	0.28	1.26	0.49	0.14
K_2O	2.77	4.12	2.66	6.6	12.03	58.40	5.04	0.08	0.04
SO_3	0.15	0.97	0.32	0.8	2.96	5.35	7.73	4.10	_
P_2O_5	0.51	01.74	1.81	0.6	_	15.23	25.60	2.44	0.23
Cl	0.092	_	_	_	_	0.68	_	_	_
MnO	_	0.35	_	_	_	0.11	2.98	0.23	0.05
MnO_2	_	_	0.83	_	_	_	_	_	_
NiO	_	0.36	_	_	_	_	_	0.22	_
ZnO	_	_	_	_	_	0.06	0.18	0.63	_
Rb_2O	_	_	_	_	_	0.05	_	_	_
CuO	_	_	_	_	_	0.02	0.14	0.18	_
SrO	_	_	_	_	_	0.02	_	_	_
CdO	_	_	_	_	_	_	_	2.47	_
Cr_2O_3	_	_	_	_	_	_	_	0.83	_
PbO	_	_	_	_	_	_	_	0.10	_
As_2O_3	_	_	_	_	_	_	_	0.03	_

Reference	Deng et al. (2013)	Ni et al. (2022)	Liu et al. (2022b)	Wu et al. (2019)	Wang et al. (2021a)	Liu et al. (2020)	Cai et al. (2021)	Cai et al. (2021)	Huang et al. (2018)
	Refuse derived fuel and other wastes								
	Antibiotic filter residue	Municipal solid waste	Refuse derived fuel						
Approximate analysis (wt%, ad)									
M	18.50	3.12	3.18						
A	12.83	16.23	9.85						
V	61.70	68.60	78.38						
FC	6.97	11.85	8.59						
Ultimate analysis (wt%, ad)									
C	32.20	42.43	44.7						
H	3.25	4.61	5.33						
O	27.65	51.32	49.5						
N	5.14	1.64	0.42						
S	0.43	0.10	0.05						
Components of ash (wt%)									
SiO_2	8.85	40.09	30.15						
Al_2O_3	8.23	9.21	9.32						
Fe_2O_3	4.97	1.39	4.24						
TiO_2	0.57	0.7	2.18						
CaO	64.66	28.6	43.56						
MgO	2.56	1.12	0.92						
Na_2O	2.07	1.17	3.39						
K_2O	3.51	4.87	0.86						
SO_3	4.58	3.04	1.58						
P_2O_5	_	5.71	1.76						
Cl	_	_	_						
Cl_2O	_	3.75	1.09						
Cr_2O_3	_	0.09	0.48						
MnO	_	0.13	0.07						
CuO	_	0.05	0.26						
ZnO	_	0.09	0.15						

Reference	Wang et al. (2021a)	Yang et al. (2022)	Yang et al. (2022)

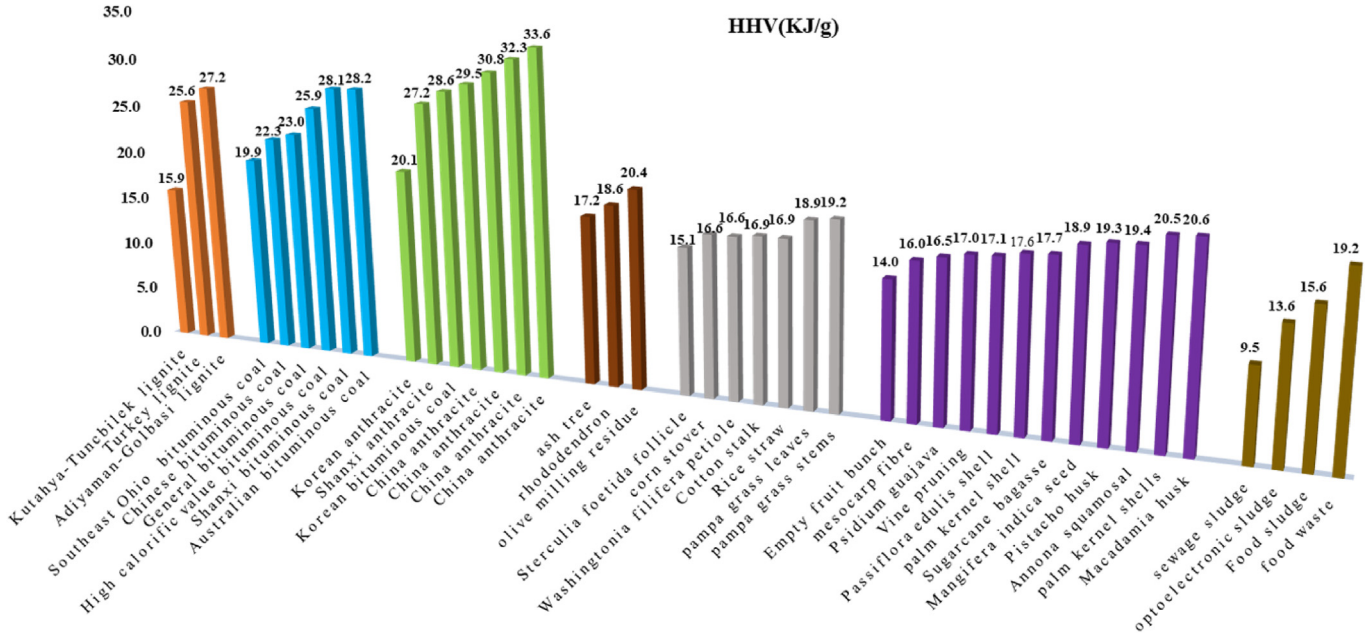

Fig. 2. The higher heating value of different coals and biomasses (Abdullah et al., 2017; Akhtar et al., 2017; Asadullah et al., 2014; Demirbas et al., 2008; Duan et al., 2012; Haykiri-Acma et al., 2016; Ikeda et al., 2003; Junga et al., 2020; Kim et al., 2007; Liang et al., 2022; Lin et al., 2021a, 2021b, 2022; Lin & Zheng, 2021; Liu et al., 2018; Mazumder et al., 2022; Otero et al., 2007; Pérez et al., 2021; Soka & Oyekola, 2020; Torres et al., 2021a; Uguz et al., 2020;Yang et al., 2021a; Zheng et al., 2020; Zhuang et al., 2019).

other waste biomass are more than that of the first three types of biomasses, including CdO, Cr_2O_3, PbO, As_2O_3, etc. Among different types of biomasses, ligneous materials, herbs and other annual plants and agricultural by-products and wastes possess higher calorific value while refuse derived fuel has less calorific value. The higher heating values of sewage sludge is only 9.48 kJ/g while that of Macadamia husk is 20.58 kJ/g, which indicates sewage sludge may be not advantageous as the potential bio-energy for co-firing in coal-fired power plants.

The proximate and ultimate analysis between different coals varied significantly, but the difference in ash content is marginal. In the proximate analysis of coal, lignite has highest ash, and relatively lowest fixed carbon compared with other two types of coals. Compared with lignite, the ash content of bituminous coal is lower and the fixed carbon content is richer. Anthracite has the highest fixed carbon content and the lowest volatile matter content. In the ultimate analysis of coal, lignite has a high proportion of C and O. The proportion of C content in bituminous coal and anthracite is higher than that in lignite, while the proportion of O content is lower. In the analysis of coal ash, it can be found that the ash components of three types of coal are mainly SiO_2 and Al_2O_3. In generally, the higher heating value of lignite is the lowest, followed by bituminous coal, and that of anthracite is the highest.

3. The co-firing behavior of coal with biomass

Compared with coal, biomass had different properties such as lower calorific value and higher volatile matter. The lower calorific value of biomass generated the less heat energy, which might lead to the lower temperature of water wall. The higher volatile matter in biomass would make ignition easier, thus the ignition temperature was lower (Cai et al., 2014). In addition, due to the difference between coal and biomass, when coal and biomass are combusted together, the combustion behavior is not a simple superposition of coal combustion and biomass combustion. There are complex interactions between coal and biomass during the co-firing process. Therefore, to better understand the co-firing of coal and biomass, the following paragraphs would gradually discuss the co-firing indices, co-firing mechanism, and synergistic effects in sequence.

3.1. The co-firing indices of coal and biomass

With the advancement of combustion research, the number of combustion indices has increased. However, ignition, burnout, and the maximum combustion rate temperature, based on monitored thermogravimeter (TG) and derivative thermogravimetry (DTG) curves, remain the primary indices for fuel combustion. The TG and DTG curves illustrate the rate of weight changes in relation to temperature or time. These indices represent the initial, final, and intermediate stages of combustion, separately, and are considered the most representative. In the following paragraphs, we will introduce these three indices and discuss how the addition of biomass to coal co-firing affects them.

3.1.1. Ignition and burnout temperature

Ignition temperature indicates the threshold of self-sustaining combustion, and a lower ignition temperature is preferred due to the ease of firing. The burnout temperature refers to the temperature at which the coal or biomass is almost combusted to form ash. A lower burnout temperature implies that the feedstock is easier to be burnt to form ash. The co-firing of coal and biomass tends to reduce the ignition and burnout temperatures compared with the firing of coal alone due to the lower ignition and burnout temperature of biomass. When Bermuda grass and corn straw biomass (20%) were mixed with bituminous coal, individually, the ignition temperature of the blends decreased by about 100 and 170 °C, respectively, compared with that of coal. The ignition temperatures of the two kinds of blends (20%) were similar to that of biomass. This was because biomasses contained plenty of easily decomposable volatile, which contributed to ignition easily. Therefore, it is a good strategy to add biomass to coal for co-firing, which would be profitable to ignition (Yu & Chen, 2016). In another study, similar results were obtained by mixing anthracite with pine wood biomass in different proportions (Wang et al., 2014). Umar et al.

(2021) also found that the reduction of ignition temperature of blends was due to the high content of volatile matter in the biomass, and the rapid volatilization and oxidation of volatile matter led to a lower ignition temperature of the mixture. In addition, compared with coal, biomass generally contains lower fixed carbon, which is a more difficult material to be ignited than volatile. The ignition indicator is conductive to study initial stage of co-firing, and the burnout indicator is vital for the final phase of co-firing. Generally, compared with coal combustion, the co-firing of coal and biomass would also decrease the burnout temperature, which is also related to the high content of volatile matter in biomass. When biomass was decomposed and the volatiles were released, and porous char was formed, which facilitates the contact between oxygen and char, leading to lower burnout temperature. In addition, the decrease of burnout temperature is also relative to the low content of fixed carbon in biomass because the fixed carbon is the main combustible material (Liu et al., 2015b).

Generally, compared with coal combustion alone, addition of biomass to coal for co-firing tends to improve the characteristics of ignition and burnout such as lowering ignition and burnout temperatures. There are various types of biomass, and thus the properties of different biomass also vary widely. When the different kinds of biomass are co-fired with the same coal, the ignition and burnout characteristics are different. A study found that at the same mixing ratios and heating rates, compared with switch grass, the beet root led to the lower ignition temperatures of co-firing with bituminous coal. The ignition temperature obviously decreased by about 200 and 110 °C when bituminous coal co-fired with beet root or switch grass of low proportion (20%) at the different heating rates, respectively. The main factor was the higher volatile matter in beet root than switch grass, which led to the lower ignition temperature. The content of volatile matter was the controlling factor, and thus the heating rates hardly affect the ignition temperature. Different from ignition temperature, the burnout temperature showed little change when adding the low proportion (10%–40%) of biomass (beet root or switch grass) for co-firing with coal at the same heating rate. This is because the content of fixed carbon is one of the main controlling factors. Compared with coal, the two kinds of biomass contained less fixed carbon. Therefore, when the low proportion of biomass was added to coal, the contents of fixed carbon in mixtures did not change too much. Hence, when biomass was mixed to coal at low proportions, there was little change in burnout temperature. However, with the increase of the heating rates, the burnout temperatures intensely increased. The main reason was the increase of heating rates contributes to the shift of DTG curves in final stage from low temperature region to high temperature region (Ahn t al., 2014; Liu et al., 2015b). Another research found that adding 20% wheat straw or corn straw to bituminous coal reduced the ignition temperature by 20 and 40 °C, respectively. The lower ignition temperature of corn straw was mainly caused by higher contents of volatile matter than wheat straw (Liu et al., 2015b). Wang et al. (2013) discovered that compared with corn straw and bark, the co-firing of corncob with coal lead to ignite much quicker and burnout more complete. It was speculated that comparing with other biomasses, the highest content of volatile in the corncob led to rapid ignition. The lowest contents of ash in corncob were less likely to block pores in the char, and thus increased the reaction surface and gas diffusion rate, which favored complete burnout. Therefore, the corncob was an excellent material to improve the ignition and burnout (Wang et al., 2013). Another work also proved that corncob contributed to the better ignition compared with hardwood. The main reason was that corncob contained more hemicelluloses and cellulose, while hardwood contained more lignin. Compared with hemicelluloses and cellulose, lignin is more thermally stable material, so hardwood was more difficult to decompose than corncob, leading to its higher ignition temperature (Liu et al., 2016b). In addition to the inherent properties of biomass, experimental operation conditions also impacted co-firing performance. Zhang and Lu (2013) conducted experiments on the co-firing of three types of coal and one type of biomass and found that the ignition temperature and maximum combustion rate temperature increased significantly with the increase of particle size of mixtures. The probable reasons were that during the heating process of larger particles, the internal heat conduction might be the limiting factor. This could potentially slow down the release rate of internal volatiles, thereby increasing the ignition temperature. In addition, larger particles had smaller specific surface area, which might affect the speed at which oxygen diffuses into the particles, further enhancing the ignition temperature (Zhang & Lu, 2013). Burnout efficiency generally referred to the completeness of the combustion process. High burnout efficiency meant that the fuel had been fully combusted, with minimal unburnt residues. The ignition temperature of blends (coal and olive waste) increased and burnout efficiency decreased when CO_2 replaced N_2 in air. The reason was probably the higher specific molar heat of CO_2. “Specific molar heat” referred to the amount of heat absorbed or released in unit mole substance with unit temperature variation. Compared with N_2, the higher specific molar heat of CO_2 meant that it needed to absorb more heat to increase its temperature. Therefore, when CO_2 was used instead of N_2, more heat was needed to reach the ignition temperature, which may lead to an increase in ignition temperature and a decrease in burnout efficiency. Additionally, it was also found that the ignition temperature decreased and burnout efficiency increased with the increase in oxygen. The main reasons were that higher contents of O_2 to the surface of blends easily contributed to volatilization and combustion of volatile. In addition, due to the increase of O_2, more char could be completely combusted leading to the enhancement of burnout efficiency (Riaza et al., 2012).

3.1.2. The maximum combustion rate temperature

The maximum combustion rate temperature refers to the temperature at which the combustion rate reaches its maximum during the combustion process. A lower maximum combustion rate temperature might imply a higher reactivity of reactant, meaning it can reach its maximum combustion rate at a lower temperature. This could be due to the organic components in the fuel undergoing rapid thermal reaction in the atmosphere at lower temperatures, and releasing a large amount of heat. In general, the addition of biomass tends to higher maximum combustion rate temperature. When bituminous coal or sub-bituminous coal was co-combusted with 20% pine sawdust, the ignition temperature reportedly decreased while the maximum combustion temperature rose, in comparison to combustion of coal only. The reason was the high volatile content in wood biomass led to rapid desorption of the light hydrocarbon in the char in the initial stage, thus in the latter char combustion stage resulting in less reactive combustible reactants in the char (Ahn et al., 2014). Similarly, the maximum co-firing temperature of the high alkali coal and municipal sludge increased with municipal sludge proportion. The main reason was that the thermal decomposition of stable inorganic components in municipal sludge was difficult, which led to the low reactivity (Wang et al., 2022).

3.1.3. The main factors and improvement strategy for combustion indices

The factors influencing combustion indices are crucial in selecting the appropriate types of biomass and operating conditions. Therefore, in addition to the proportion of biomass mentioned above, which has a significant impact on ignition, the various organic and inorganic components in the biomass also have

a significant impact on combustion indices. A study found that the contents of the cellulose, xylan and lignin affected co-firing of the blends of coal and corn straw. When cellulose and xylan increased, the maximum volatilization and combustion rate of volatiles increased while temperature range of char combustion was almost unchanged, which suggested that cellulose and xylan contributed to the ignition but had no significant effect on the combustion of char. However, the addition of lignin promoted the maximum combustion rate of char. Therefore, when biomass contained more cellulose and xylan, the ignition was easier. When biomass contained more lignin, the char combustion tended to be quicker (Kai et al., 2011). Apart from the organic components, minerals in biomass ash also affected the co-firing of coal and biomass. The minerals present in rosewood inhibited the volatilization process, which led to higher temperature in volatilization and ignition delay. However, some minerals showed positive effect on the co-firing. Minerals such as Ca, K_2O and Cl could act as catalyst for char combustion (Shi et al., 2019).

Therefore, in order to increase both the ignition and char combustion rate, biomass with multiple types can be selected for a certain proportion of mixing, thus forming excellent composite biomass materials. In addition, pretreatment methods for biomass such as washing or hydrothermal carbonization had impacts on the co-firing of coal and biomass. After washing and hydrothermal carbonization of wheat straw, the maximum combustion temperature decreased and the maximum combustion rate increased for blends of 40% coal and wheat straw, which was caused by the breaking of cellulose, hemicellulose and lignin structures (Ma et al., 2022).

3.2. The co-firing mechanism of coal and biomass

Besides co-firing indices, it is essential to study the co-firing mechanism of coal and biomass. This is because the co-firing mechanism of coal and biomass is crucial for understanding the main limiting factors on co-firing reaction rates of each stage according to TGA curves. Basically, coal and biomass are solids, and the combustion follows basic solid reactions models listed in Table 4. The main influencing factors of co-firing mechanism include the mixing ratio and the heating rate. Gil et al. (2010) heated the mixture of bituminous coal and pine sawdust in air from room temperature to 1000 °C at a heating rate of 15 °C/min. According to TG and DTG curves, the combustion stage of the blends was divided into three stages: the release and combustion of biomass volatiles (stage A), the combustion of fixed carbon in biomass (stage B) and the combustion of fixed carbon in coal (stage C). It was found that the stage A and stage C were controlled by the first-order kinetics model (O1), which indicated that the rates of stage A and C was determined by the remaining fraction of reactant. The stage B was controlled by the diffusion mechanism of 3D diffusion-Jander's equation (D3) and Ginstling–Brounshtein's equation (D4), which implied that diffusion of oxygen into the particle was the rate controlling step rather than chemical reaction (Gil et al., 2010). In another study, the bituminous coal was co-fired with composite biomass including wood waste, rice straw and catkins, and DTG curves were measured. Subsequently, similar combustion stages and combustion mechanisms were observed. The difference was that this study stated that stage B was controlled by the diffusion mechanism of D1 rather than D3 and D4. The study also found that when the same composite biomass was co-combusted with lignite there were only two combustion stages: combustion of volatile in lignite and biomass, and the combustion of char in lignite and biomass. These two stages were only controlled by D3 and D4 diffusion mechanisms, indicating that the co-firing of lignite and the composite biomass was controlled by the process of oxidant diffusion to the reaction particles. Therefore, the study demonstrated that different coal types lead to different reaction mechanisms (Guo et al., 2020). In addition, another study also found that the co-firing mechanism of each stage for blends of refuse-derived fuel and low-quality coal was controlled by the D3 diffusion model, and thus oxygen transfer rate was the key for the co-firing of coal with refuse-derived fuel (Isaac & Bada, 2020). The above-mentioned studies are based on Coats–Redfern linear fitting method to obtain the co-firing mechanism. Although the co-firing mechanisms tested in the above experiments considered the influence of biomass proportion in the mixed fuel, these studies did not consider the influence of heating rate. Actually, the heating rate is also a key factor influencing the co-firing process. Liu et al. (2015a) not only studied the influence of mixture ratio but also considered the effects of different heating rates on the co-firing mechanism of coal and beet root. Using the two-stage theory, the co-firing process was divided into two stages. The main combustion mechanism of the two stages in coal/beet root blends was described by Avrami–Erofeev's equation. It meant that the reaction rate was controlled by the process of random nucleation and growth, referring to the process during a phase transition where the formation of a new phase began with the spontaneous formation of small clusters (or "nuclei"). Therefore, the formation and growth rates of new phases (such as gaseous products or newly formed solid materials) during the co-firing of coal and beet root were key factors influencing the reaction rate.

Table 4
Expressions of $g(x)$ for the kinetic model functions usually employed for the solid-state reactions (Gil et al., 2010).

Reaction order	Mechanism and model	
	$g(x)$	$f(x)$
First-order (O1)	$-\ln(1-x)$	$(1-x)$
Second-order (O2)	$[1/(1-x)]^{-1}$	$(1-x)^2$
Third-order (O3)	$(1/2)\,[(1-x)^{-2}-1]$	$(1-x)^3$
Diffusion		
1-D diffusion (D1)	x^2	$1/(2x)$
2-D diffusion (D2)	$(1-x)\ln(1-x)+x$	$-[1/\ln(1-x)]$
3-D diffusion-Jander (D3)	$[1-(1-x)^{1/3}]^2$	$[3(1-x)^{2/3}]/[2(1-(1-R)^{1/3})]$
Ginstling–Brounshtein (D4)	$1-(2/3)x-(1-x)^{2/3}$	$3/[2((1-x)^{-1/3}-1)]$
Nucleation model		
Avrami–Erofeyev (A2)	$[-\ln(1-x)]^{1/2}$	$2(1-x)[-\ln(1-x)]^{1/2}$
Avrami–Erofeyev (A3)	$[-\ln(1-x)]^{1/3}$	$3(1-x)[-\ln(1-x)]^{2/3}$
Avrami–Erofeyev (A4)	$[-\ln(1-x)]^{1/4}$	$4(1-x)[-\ln(1-x)]^{3/4}$
Phase boundary-controlled reaction		
Contracting area (R2)	$1-(1-x)^{1/2}$	$2(1-x)^{1/2}$
Contracting volume (R3)	$1-(1-x)^{1/3}$	$3(1-x)^{2/3}$

3.3. The interaction between coal and biomass during co-firing

After understanding the co-firing indices and mechanisms based on TGA curves, the synergistic or antagonistic effects during different combustion stages based on TGA curves are worth studying, favoring for selecting appropriate types of coal and biomass. The performance of co-firing of coal and biomass is not simply a mathematical superposition of some percentage of coal and some percentage of biomass. The correlation of co-firing is non-linear which shows synergistic effects or antagonistic effects. The co-firing test of 70% lignite and 30% cardoon was performed in a thermo-gravimetric analyzer. The results indicated that the co-firing rates of blend in experiment were higher than calculated co-firing rates at the major combustion zone. The calculated co-

firing rate of the blend at any instant of time or temperature was formulated by Eq. (1):

$$\left(\frac{dm}{dt}\right)_{blend} = x\left(\frac{dm}{dt}\right)_{coal} + y\left(\frac{dm}{dt}\right)_{biomass} \quad (1)$$

where, $(dm/dt)_{coal}$ and $(dm/dt)_{biomass}$ were the rates of normalized mass loss of coal and biomass, respectively, at any instant of time or temperature as found from the individual experiments, and x, y were the mass fractions of coal and biomass in the blend, respectively. The conclusions of co-firing studies implied that co-firing generated synergistic effect at the major combustion zone rather than simple superposition (Vamvuka & Sfakiotakis, 2011). Another study also reached the same conclusion during the co-firing of coal/sawdust char and coal/corn cob char by comparing experimental results with calculated values under different proportions of biomasses. The experimental combustion rates in blends were faster than the calculated combustion rates at the major combustion zone. Thus, the sawdust char and corncob char promoted co-firing at the major combustion zone. However, the effects of combustion rates at the final combustion zone were different for two types of blends. For the mixing of coal and sawdust char, the combustion rates at the final combustion zone were almost the same between experimental measurement and the calculated value by Eq. (1). While the values of combustion rates were lower in experiment than the calculated value at final combustion zone as to the mixing of coal with corncob char. This proved that sawdust char had nearly no influence on final combustion phase of the co-firing. However, corncob char performed antagonistic effects on final combustion zone (Sahu et al., 2013). When bituminous coal is co-combusted with pine sawdust and rice husk, respectively, stages of devolatilization and combustion of volatiles showed anti-synergistic effects when comparing experimental results and calculated values. The main reason was the heterogeneous particle sizes of blends influenced the thermal transmission. Nevertheless, the stage of carbon residue combustion exhibited synergistic effect in blend of coal with pine sawdust. This was because char from biomass elevated combustion of blends due to the faster ignition and release of heat in char from biomass. Another explanation was the presence of a high content of alkali as a catalyst in pine sawdust ash, which significantly promoted the combustion. However, the anti-synergistic effect of rice husk on mixing was owing to the high SiO_2 content in rice husk ash, which had an obvious inhibiting effect on combustion (Wang et al., 2016). Garcia et al. (2022) co-combusted bituminous coal with spent coffee ground and rice husk, respectively. The result indicated that the blend of bituminous coal and spent coffee ground had synergistic effect on burnout temperature due to the high content of alkali metals as catalyst in spent coffee ground ash. However, there was no obvious synergistic effect on burnout temperature for mixing rice husk. The main reason was the rice husk ash contained CaO, K_2O and SiO_2. The K_2O had a strong catalytic effect, while CaO and SiO_2 could have an inhibiting effect. Therefore, there was no apparent synergistic effect on burnout temperature (Garcia et al., 2022). Another research defined the level of synergy by the degree of synergism during co-firing of coal with sugarcane bagasse and biomass sorghum bagasse. The degree of synergism (S) was calculated by the following expression (Barzegar et al., 2022; Boumanchar et al., 2019):

$$S = \left[m_{blend} - \left(\frac{xm_{coal} + ym_{biomass}}{m_{blend}}\right)\right]100 \quad (2)$$

where m_{coal}, $m_{biomass}$ and m_{blend} were the mass loss of coal, biomass and blend, and x, y were the mass fractions of coal and biomass in the mixture, respectively. The higher degree of synergism represented a stronger synergistic effect. The result indicated that the blends of 10% and 75% biomass ratios showed a higher degree of synergism while the blends of 25% and 50% biomass ratios showed a lower degree of synergism in the oxy-fuel combustion condition compared with air combustion condition. It is worth mentioning that the mixing of coal and sorghum bagasse had the highest degree of synergism, up to 15.12 (Galina et al., 2019).

4. The ash agglomeration, fouling and slagging behaviors

Although the co-firing of coal and biomass would lead to many benefits such as lowing ignition temperature, there are many potential problems due to the differences between coal and biomass. The ash characteristics would be changed when the biomass was added to coal for co-firing in the existing coal-fired boiler, which contributed to agglomeration, fouling and slagging. When the temperature reached the initial deformation temperature, ash began to melt and form small particles or “nuclei”. These nuclei spontaneously combined to form larger particles, a process known as “agglomeration”. Over time, these particles might adhere to the interior surfaces of the boiler, forming deposits, a process known as “fouling”. If the deposits continued to accumulate and become large enough, they might melt and adhere to boiler components, forming a hard, glassy structure, a process known as “slagging”. For studying the potential of agglomeration, fouling and slagging when biomass was added to coal for co-firing, the ash melting temperatures such as initial deformation temperature, softening temperature, hemispherical temperature and flow temperature could be measured. The lower ash melting temperatures would lead to ash agglomeration, fouling and slagging. In general, the ash melting temperatures in biomass were lower than that in coal. When a low rank coal was co-combusted with biomass blends of sewage sludge and wood sawdust, the agglomeration degree of biomass ash was twice as high as that of low rank coal ash. Therefore, with the increase of biomass proportion in blend, the agglomeration degree of ash increased. The main reason was that the ash melting temperatures of biomass blend were lower than that of coal. The reason for using biomass blend instead of single wood sawdust biomass was that the aluminum, calcium and iron in the sludge could combine with the alkali metals in the woody biomass, raising the ash melting temperature (Namkung et al., 2018). For the ash in bio-coal briquette made of lean grade coal and torrefied woody biomass, the addition of a low proportion of biomass had no significant effect on agglomeration, fouling and slagging, because the ash content of woody biomass was far below that of coal. Hence, the composition change in ash of the blend was negligible. However, the addition of a high proportion of biomass produced more change in ash components, resulting in the low melting point ash of blend and a tendency to agglomerate, foul and slag (Adeleke et al., 2022). Another research studied the fouling trends of co-firing of three types of biomass with bituminous coal. The results showed that palm kernel shell and bark promoted the fouling obviously, and Japanese cedar had little effect on the fouling. This was because the co-firing of coal and palm kernel shell and bark elevated the concentration of low-melting calcium mineral (Ca–Al–Si). Palm kernel shell had a more obvious promoting effect on fouling than bark, because the iron further formed calcium mineral (Ca–Fe–Al–Si) with a lower melting point (Priyanto et al., 2018). When lignite (90%) was co-combusted with hazelnut shell (10%) or rice husk (10%) respectively, the addition of hazelnut shell led to a decrease by nearly 50% in initial deformation temperature. The probable factor was that with the increase of CaO, the initial deformation temperature first decreased and then increased. When the CaO content reached 35%, the initial deformation temperature reached

the lowest value. Therefore, the intense decrease in initial deformation temperature for blend was because the CaO content reached about 35%. However, the co-firing of lignite and rice husk only led to a minor change in initial deformation temperature. Therefore, the rice husk was a better choice to reduce the potential of ash agglomeration, fouling and slagging. The variety of biomass was extensive, and under different operational conditions, selecting the appropriate biomass for co-combustion with coal was crucial. Besides the choice of biomass, the addition of inhibitors was also highly effective in reducing the likelihood of slagging (Haykiri-Acma et al., 2010).

5. Gaseous pollutant emissions of coal and biomass combustion

Biomass is a clean fuel, tending to reduce some significant gaseous pollutant emissions such as CO, NO and SO_2. Meanwhile, the adverse effect probably takes place owing to the diversity of biomass. When cedar nut shell was co-combusted with bituminous coal or lignite, respectively, it was found that co-firing of bituminous coal and cedar nut shell significantly reduced SO_2 and H_2S emissions in flue gas, while co-firing of lignite and cedar nut shell did not substantially lower SO_2 and H_2S emissions. The main reason was lignite combusted earlier than cedar nut shell. Then ash of cedar nut shell formed too late so that the sulfur in lignite could not bind with mineral compounds in the ash of cedar nut shell. The latest research found cedar nut shell could remarkably reduce the content of SO_2 during combustion of bituminous coal by experiments. The main reason was that bituminous coal was combusted later, so the sulfur from bituminous coal was in contact with the mineral compounds in ash of cedar nut shell (Jerzak et al., 2018). Nevertheless, the actual measurement in boiler tended to reflect more accurate circumstances. Another study measured the gaseous pollutants produced from industrial boiler during co-firing of hard coal with wood chips. The result discovered that the content of SO_2 in flue gases decreased with addition of wood chips, due to high sulfur content in hard coal and low sulfur content in wood chip. In addition, the study found that the content of VOC and HCl decreased while the amount of CO_2 and NO_x increased in flue gases with the addition of wood chips (Nowak & Rabczak, 2021). At the same time, another study also showed that the co-firing of anthracite and wood pellets would reduce the emission of SO_2, compared with the combustion of anthracite alone (Guo & Zhong, 2018). The reason was that wood pellets contained many alkali and alkali-earth minerals, which would form sulfate with SO_2. Biomass-char could act as a catalyst for the sulfating reaction. Besides, the research also found that the addition of wood pellets led to a decrease in the content of NO and an increase in the content of CO. The reasons were that the nitrogen content in wood pellets was low and there was not enough air at the bottom to burn wood pellets, which caused incomplete combustion to produce a large amount of carbon monoxide (Guo & Zhong, 2018). The co-firing of lignite and different biomasses led to the decrease of NO_x compared with combustion of lignite. However, the nitrogen content in these biomasses was higher than lignite. The main reason for NO_x decrease was that the char content in biomasses was higher than lignite, and the char could act as a catalyst in reducing NO to N_2. In addition, the co-firing also reduced SO_2 concentration due to the low sulfur content in biomasses (Krzywanski et al., 2014). Patil et al. (2022) considered that the biomass mixing ratio influenced the combustion of coal. With the increase of the distillery sludge ratio, the co-firing of blends would generate more SO_2 in the flue gas, which was attributed to the high sulfur content in sludge. This is because the distillery sludge contained abundant protein amino acid with sulfur moiety. Yet, the NO_x concentration decreased in flue gas with an increase in the ratio of sludge. Although the nitrogen content of blends was higher than coal, the nitrogen element existed as fuel-N in a more stable form in blends, thus the NO_x in flue gas was more difficult to form in blends (Patil et al., 2022). The co-firing experiments of bituminous coal and poplar wood also presented the phenomenon that the NO yield decreased with the increase of the poplar wood ratio because of the low nitrogen content in poplar wood. In addition, the research also found that the NO yield in O_2/N_2 atmosphere was far lower than O_2/H_2O atmosphere for the co-firing experiment. One of the reasons was that the concentration of reducing gases such as H_2 and CO and free radicals increased in O_2/N_2 atmosphere, favoring the NO reduction to form N_2 (Li et al., 2018). Apart from the mixing ratio, the temperature was a critical factor in gaseous emissions. When the temperature was elevated, the NO concentration rose during co-firing of coal with wheat straw. The content of CO decreased due to the improvement of combustion efficiency with the increase in temperature. The tendency of SO_2 change was complex with the enhanced temperature. The content of SO_2 increased from 750 °C to 850 °C because the S in FeS_2 was oxidized to form SO_2. Then the SO_2 decreased from 850 °C to 900 °C, which was attributed to the consumption of SO_2 to form sulfate. When the temperature was elevated from 900 °C to 950 °C, the SO_2 rose again, because the sulfation was slower than the decomposition of sulfate (Xue et al., 2020). In terms of overall trends, another research also showed a similar effect of temperature on NO, CO and SO_2 emissions during co-firing of coal and rice husks (Akhtar et al., 2018). In addition, the mixing ratio should be considered as another vital factor in flue gas behavior. The CO production decreased with the increase of rice husk content adding to Lakhra coal, because the high content of volatile matter and the presence of oxygenates in rice husk would contribute to the conversion of CO to CO_2. The high content of biomass in the blends led to the reduction of SO_2, because there was almost no sulfur in rice husk and the presence of CaO led to the conversion of SO_2 to $CaSO_4$. The high content of rice husk in the mixture reduced NO_x emissions, because rice husk generated more free radicals to convert NO_x into N_2 (Akhtar et al., 2018).

6. The effect of different operations on co-firing of coal with biomass

Biomass generally has lower calorific value, energy density and larger size, which lead to challenges of co-firing in coal-fired power plants. Therefore, to deal with these problems, many researchers have provided some methods such as torrefaction, adjustment of mixing ratios and oxygen concentration, which will be stated in the following section.

6.1. Biomass torrefaction

Raw biomass with high proportion was fed into the coal-fired power plant, which would cause unstable combustion since raw biomass was a fuel of low calorific value and difficult to pulverize. To overcome this, biomass was torrefied at certain temperatures which would enhance its calorific value and pulverizibility. Compared with raw biomasses (willow, olive oil residue and waste wood), torrefied biomasses improved higher heating value, which would be favorable to co-firing. In addition, torrefied biomass forfeited a part of moisture and volatile matter, which would reduce the weight of biomass to diminish the costs of transportation (Kopczyński et al., 2017). With the increase in torrefaction temperature from 200 °C to 300 °C, higher heating value of both healthy pine and beetle kill pine increased by 19.27% and 17.80%, respectively. In addition, the particle sizes of biomass after milling were smaller at higher torrefaction temperatures. The main reason

was that the decomposition level of hemicellulose, cellulose, and lignin of biomass was higher at higher temperatures (Howell et al., 2018). Another study also found the particle size of torrefied biomass was smaller than raw biomass and the size further decreased as the torrefaction temperatures increased (Gil et al., 2015). According to the DTG curves, there were three peaks for the combustion of raw bamboo while there was a single peak for combustion of coal or torrefied bamboo at 20 ml/min and 40 ml/min air flows, which indicated there were similar combustion behaviors between coal and torrefied bamboo. The reduction in the number of combustion peaks for torrefied bamboo was due to the evaporation of water and the decrease of volatiles to a similar level as coal after torrefaction. In addition, the heat value of bamboo increased by 8.57 kJ/g after torrefaction. Therefore, torrefied bamboo was potentially to be an alternative as the substitute for coal in the coal-fired boiler (Liu et al., 2016a). When three types of coals (lignite, bituminous coal and anthracite) with torrefied cornstalk were co-fired, the peak values of volatilization increased with the blending ratios of torrefied cornstalk because the volatile content of torrefied cornstalk was higher than that of coals, resulting in the improvement of ignition temperature. Besides, compared with the blends of lignite/bituminous coal and torrefied cornstalk, the co-firing of torrefied cornstalk with anthracite had more peaks in DTG curves owing to a difference of combustion temperature ranges between torrefied cornstalk char and anthracite char. The increase in peak numbers resulted in the discontinuity of co-firing in coal-fired boiler. Therefore, lignite and bituminous coal were more appropriate than anthracite, when co-firing with torrefied cornstalk (Liu et al., 2022b). In addition to the number of combustion peaks, the thermogravimetric analysis was used to study the interaction between coal and torrefied biomass. When coal was co-combusted with torrefied biomass (agricultural and animal wastes), there were obvious synergistic effects in terms of lower burnout temperature. The reason might be that the inorganics in the biomass acted as a catalyst in the final combustion processes (Toptas et al., 2015).

6.2. The coal and biomass coupling power generation technology

To alleviate the various pollution problems such as SO_x and NO_x emissions caused by coal-fired power, the coal and biomass coupled power generation technology is the primary method and increasingly developing. According to the co-firing mode, the coal and biomass coupled power generation technology is mainly divided into direct, indirect, and parallel co-firings (Agbor et al., 2014).

6.2.1. Direct co-firing

For direct co-firing, there were two ways in which coal and biomass enter into coal-fired boiler. The first way was that the coal and biomass were mixed, then ground together, and finally fed into the coal-fired boiler (Fig. 3(a)). The second method was that the coal was entered into the grinder while biomass got into the newly established biomass grinder, then ground coal and biomass entered the coal-boiler together (Fig. 3(b)). The crushing characteristics of biomass differed greatly from those of coal. Hence, the coal mills, which are primarily designed for grinding and crushing coal, were not up to the task of cracking the fibers in biomass containing high cellulose content. To increase the co-firing ratio of biomass, special biomass mills should be developed, but this would increase retrofitting costs (Wang et al., 2021b). Although the installation of a specialized biomass mill would alleviate uneven feeding issues, the direct co-firing encountered other problems such as corrosion. The produced deposits from co-firing of 25% woody biomass with 75% coal in a 150 MW pulverized-coal boiler contained more alkali sulfate and more unburned carbon compared with that from co-firing of coal alone. The substantial unburned carbon formed a reducing atmosphere, which increased the generation of H_2S. The presence of both alkali sulfate and H_2S resulted in corrosion in the

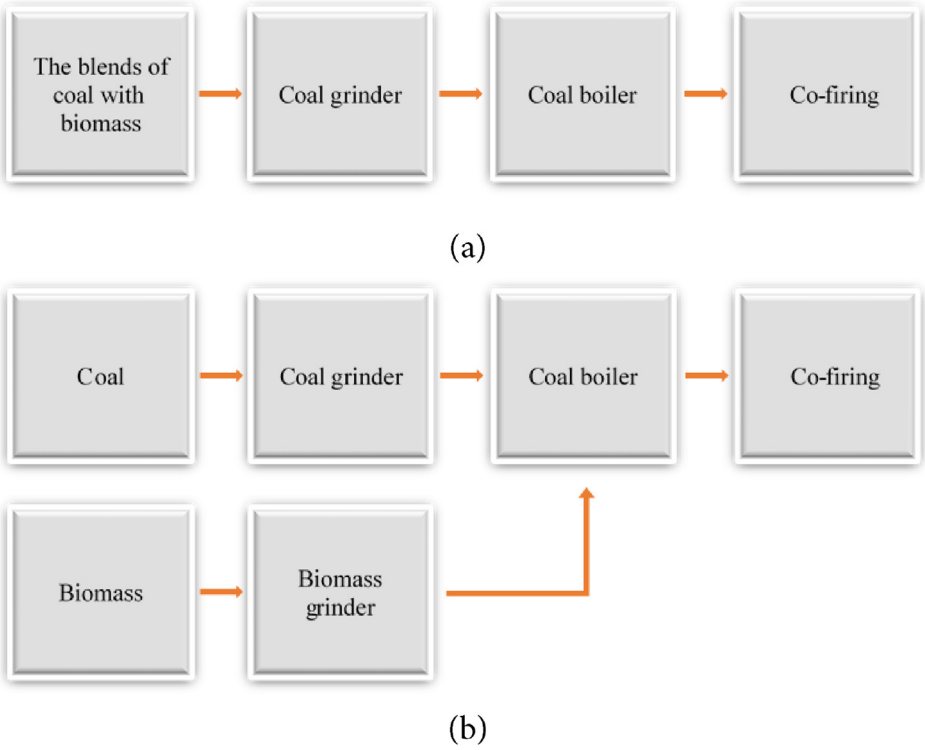

Fig. 3. (a) The blends of coal with biomass into the same grinder for direct coupling; (b) The coal and biomass into the different grinder for direct coupling.

furnace chamber. One method for minimizing corrosion was to alter the air ratio to limit the reducing atmosphere (Priyanto et al., 2017). Another industrial boiler of long-term operation also reported corrosion issues. An 80 MW circulating fluidized bed boiler with 50% straw and 50% coal ran normally for 6 months at less than 80% combustion chamber load, but serious corrosion occurred in the final superheater one year later (Hansen et al., 1998). For co-firing of bituminous coal and straw pellets in a 260 t/h CFB boiler, the substantial release of gas phase chlorine from the process of sulfation of potassium chloride in the sediments was the primary source of corrosion. In addition to corrosion, because the ash melting point of biomass waste was lower than that of coal, direct co-firing for coal and biomass waste would result in more slagging. However, directly coupled combustion of coal with biomass waste lowered NO_x and SO_2 levels in the flue gas. The decrease in NO_x content was mostly attributable to the reducing environment in the furnace, which reduced NO_x to N_2. The drop in SO_2 amount was mostly owing to the low S content in biomass waste and the combination of SO_2 with the minerals in the ash to generate sulphates. Compared with indirect and parallel co-firing, direct co-firing is prone to slagging and corrosion, but it has the lowest investment cost for retrofitting. Therefore, direct co-firing was the most common commercial technology for co-firing coal and biomass in a boiler (Liu et al., 2021).

6.2.2. Indirect co-firing

The indirect co-firing involved feeding biomass into a gasifier for gasification. The gas product generated from gasifier was used as fuel for coal-fired boiler (Fig. 4). Compared with direct co-firing, indirect co-firing reduced the problems such as slagging in the furnace chamber and thus enhancing biomass mixing ratio can be achieved (Xu et al., 2020). When bio-gas of different mass percentages (3%–50%) were co-fired with coal in a 600 MW coal-fired boiler, it was found that when the mass percentage of bio-gas was increased to 50%, all particles in the furnace were burned completely. In addition, the study showed that as the proportion of biomass gas increased, the average temperature along the chamber height and the NO content at the flue gas outlet decreased, but the CO and CO_2 content did not change significantly. The high mass percentage of biomass gas significantly reduced slagging due to the reduced temperature in the furnace chamber (Jiang et al., 2009). Despite many advantages, indirect co-firing was not widely used commercially in many regions due to the high investment costs required for the additional gasifier.

6.2.3. Parallel coupling

For parallel co-firing, coal and biomass were pre-treated separately in dedicated coal and biomass pre-treatment systems before being burned separately in coal-fired boilers and biomass-fired boilers, respectively (Fig. 5). Compared with indirect co-firing, the parallel co-firing further enhanced the biomass mixing ratio and the stability of the combustion operation, as well as further reducing slagging and corrosion problems. However, the investment costs were the highest due to the need for an additional dedicated biomass system. Therefore, the parallel co-firing had few commercial applications (Agbor et al., 2014).

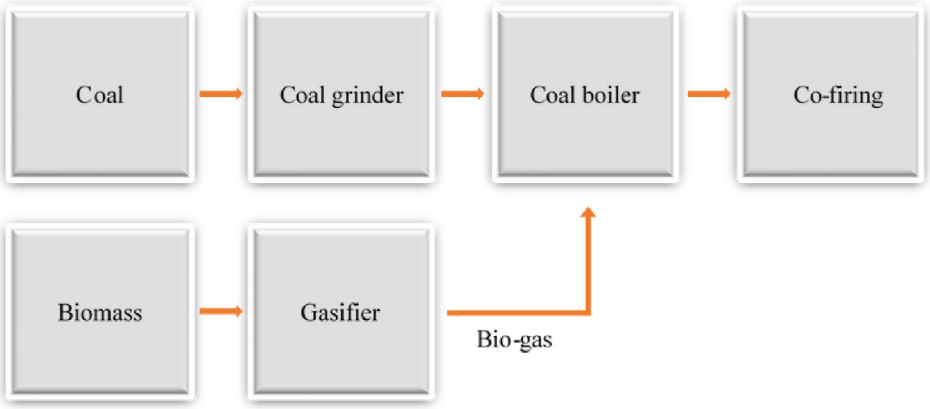

Fig. 4. The coal and bio-gas into the boiler for indirect coupling.

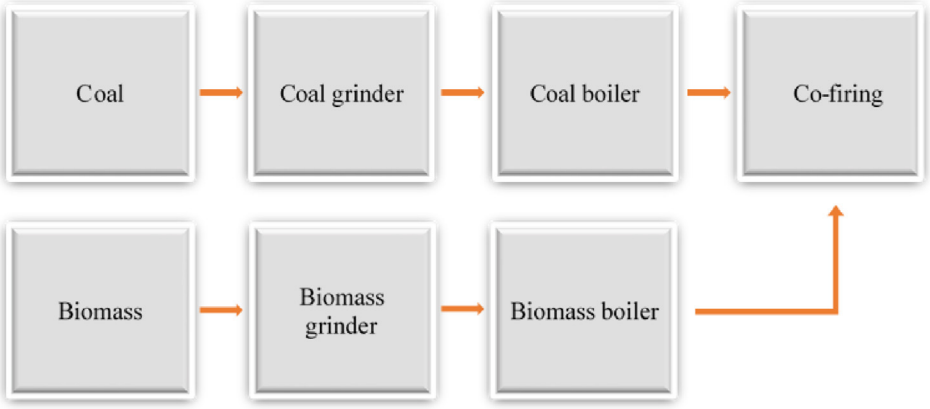

Fig. 5. The coal and biomass into the boiler for parallel coupling.

6.3. The effect of co-firing ratios

Due to the difference in combustion characteristics between coals and biomasses, the co-firing ratio had a major impact on the generation of pollutants, production heat of the boiler and corrosion in boiler when coal and biomass were co-fired together in existing pulverized coal boilers. A study on co-combusted coal and pine sawdust with various mixing ratios demonstrated that with the increase of pine sawdust proportion, despite an increase in released volatiles, the maximum NO concentration gradually reduced from 62 ppm to 48 ppm in the stage of devolatilization. The low nitrogen content in pine sawdust is one direct reason for the low NO emission, and the high volatiles in pine sawdust consumed oxygen and created a locally reducing environment, which favored the conversion of NO to N_2 (Yang et al., 2021b). In order to obtain the optimum mixing ratio for minimizing gaseous pollutant emission for different biomasses, coal was co-combusted with biomass of four types at different co-firing ratios. For minimum CO emission, the optimum biomass blending ratios were 50%, 30%, 30% and 30% for poplar sawdust, rice husk, sunflower leftovers and pine nuts shell, respectively. For minimum NO_x emission, the optimum biomass blending ratios were 30%, 20%, 30% and 50% for the above biomasses. In addition, for minimum SO_2 emission, the optimum biomass blending ratios were 50%, 40%, 30% (or 50%) and 50% for the above biomasses. The emission of all the above gaseous pollutants would reach the minimum value when coal was co-combusted with 30% sunflower leftovers. Therefore, to reduce pollution, the most appropriate biomass was sunflower leftovers and the most the optimum biomass blending ratio was 30% (Kanwal et al., 2021). Due to the higher fraction of volatiles in biomass, when burning coal and municipal solid waste together, NO and CO levels in the flue gas rose with the proportion of biomass. However, as the ratio of biomass grew, the concentration of SO_2 in the flue gas declined, mainly because coal contained a higher S content than biomass, and the biomass ash contained CaO and MgO, which absorbed SO_2 to form sulfates (Zhakupov et al., 2022). South African coal or Columbian coal and straw were co-combusted by experiment and calculations. As straw blending ratio on an energy basis increased from 0% to 70% for the co-firing of South African coal and from 0% to 50% for the co-firing of Columbian coal, the content of HCl also increased. The explanations were that gaseous alkali chlorides reacted with sulfur oxides and alumina-silicates by the following reactions: Eqs. (3)–(5):

$$2MCl(g) + SO_2(g) + 0.5O_2(g) + H_2O(g) \rightarrow M_2SO_4(g) + 2HCl(g) \quad (3)$$

$$2MCl(g) + SO_3(g) + H_2O(g) \rightarrow M_2SO_4(g) + 2HCl(g) \quad (4)$$

$$2MCl(g) + H_2O(g) + Al_2O_3 \cdot xSiO_2(s) \rightarrow M_2O \cdot Al_2O_3 \cdot xSiO_2(s) + 2HCl(g) \quad (5)$$

where M is Na or K (Wolf et al., 2017). The addition of biomass led to a reduction in boiler heat production. When lignite or bituminous coal was co-combusted with four types of biomasses (rice husk, sawdust, chicken litter, refuse derived fuel). With the increase in the biomass ratio, the produced heat of boiler decreased. The main reason was that biomass had a lower heating value than coal (Mehmood et al., 2012). Furthermore, the addition of biomass also led to corrosion. When straw was co-combusted with South African coal, Columbia coal or El Cerrejon coal in lab scale tests, respectively, as the straw blending ratios increased, the corrosion signal values and Cl content in fly ash increased, but the Al_2O_3 content decreased in blends ash. Therefore, the high Cl content and the low Al_2O_3 content in ash would lead to more severe corrosion (Stephan et al., 2017).

6.4. The effect of oxygen concentration

In addition to the biomass blending ratio, the oxygen concentration would significantly affect the co-firing performance of coal and biomass. The composite combustion characteristic index S is a comprehensive parameter to evaluate the ignition and burning performance, which is calculated by Eq. (6):

$$S = \frac{DTG_{max} \times DTG_a}{T_i^2 \times T_b} \quad (6)$$

where DTG_{max} (°C/min) is the maximum rate of weight loss, DTG_a (°C/min) is the average rate of weight loss between the ignition point and the burnout point, T_i (°C) is the ignition temperature, and T_b (°C) is the burnout temperature. A higher value of S indicates better combustion performance. When bituminous coal and wood chips were burned together, the value of S was not significantly affected by an increase in oxygen concentration from 5% to 30% when the proportion of wood chips was less than 50%. The possible reason was that the low mixing ratio of wood chip produced a low amount of volatile in the mixture of bituminous coal and wood chip, which was the main restricting factor on the combustion performance rather than oxygen concentration. However, when the blending ratio of the biomass exceeded 50%, with the increasing of oxygen concentration, the combustion performance considerably improved as the value of S increased. It demonstrated that oxygen content acted as the limiting factor with biomass of high proportion (Chen et al., 2020). When 50% coal semi-char and 50% straw were co-combusted together, the ignition temperature and burnout temperature decreased and the value of S increased as the oxygen concentration rose from 21% to 40%, which indicated that the high oxygen concentration positively contributed to ignition, burnout and combustion. Oxygen concentration played different roles in the different co-firing stages. The increase in oxygen concentration did not significantly alter the combustion rate in the devolatilization and combustion stage of volatiles for the co-firing of 70% coal and 30% pine sawdust. The increase in oxygen content, however, significantly accelerated the combustion reaction rate during the stage of stable char combustion. The combustion reaction rate in the stable char stage increased by nearly 126% when the oxygen content was raised from 6% to 21%. The main reason was that the oxygen was sufficient at the initial devolatilization and combustion stage of volatiles, then the oxygen was consumed by volatile matter, finally, the lack of oxygen contributed to limitations on the combustion rate at the final stage of char combustion (Yang et al., 2021b). It was discovered that a rise in oxygen concentration resulted in an increase in the concentration of arsenic in the ash when bituminous coal and rice husk were co-combusted under air and 70% oxygen concentration. The primary cause of this might be that increased oxygen concentration resulted in higher adiabatic flame temperatures, which vaporized particles in the ash with larger specific surface areas and more sites for arsenic to be adsorbed. As a result, in an oxygen-rich environment, the ash had a high arsenic level (Liu et al., 2020b).

7. Numerical simulation of co-firing of coal and biomass

The above experimental studies can only measure the parameters of interest at limited locations such as inlet, outlet and fixed points in the boiler. The detailed flow, heat and mass transfer characteristics, reaction rates and component concentration of co-

firing for coal with biomass inside the boiler could not be fully obtained by experimental measurement. To overcome this limitation, it is essential to develop multi-phase flow models for the gas-solid flow, temperature and gas distribution inside the boiler by means of numerical simulations.

7.1. The gas-solid flow of co-firing

For the co-firing of coal and biomass, gas-solid flow characteristics are essential for understanding the interaction between the particle and the gas. Experimental measurements only obtain a general trend of the gas-solid flow. However, the detailed distributions of the parameters influencing the gas-solid flow (particle velocity, volume fraction, etc.) inside the furnace were not known. Therefore, the numerical simulation investigated the gas-solid flow profile inside the furnace by building a multiphase flow model. A model using the Eulerian−Lagrangian framework simulated the co-firing of coal and biomass in a fluidized bed. The results showed a common three-zone flow pattern. According to particle concentration, the fluidized bed along the bed height was divided into three zones: a dense phase zone and a splashing zone at the lower part including almost all particles, and a dilute phase zone at the upper region, which barely contained particles (see Fig. 6). The particles in the dense phase and splashing zones exhibited annular-core structure, with higher particle velocity but lower particle concentration in the central region and lower particle velocity but higher particle concentration around the walls. The distribution of the velocity and concentration of particle was uneven in the dense phase zone, which was caused by the movement of bubbles including bubbling generation, bubble aggregation and bubble fragmentation. However, the particles including biomass, coal and inert bed material were mixed well in the dense phase and particle splashing zones due to sufficient bubbling velocity. In addition, compared with combustion of coal, addition of biomass led to an increase in bed height of the dense phase and e-splashing zones. The main reason was that due to the low calorific value of the biomass, more particles were fed into the fluidized bed to keep the bed temperature constant. Co-firing also caused the increase in particle velocity owing to the low mass density of biomass (Liu et al., 2020a;Liu et al., 2022a). Another study simulated the co-firing of coal and sludge in a circulating fluidized bed by the Eulerian−Lagrangian method (Wu et al., 2023). The particle flow behaviors of different particle sizes in a circulating fluidized bed at the same simulation time were investigated. When the size of the particle was 0.1 mm, the particles flowed quickly in the whole circulating fluidized bed. However, in the case of particle size of 1 mm, the particles accumulated at the bottom of the furnace and flowed slowly. Therefore, compared with large particles, small particles led to greater flow in the circulating fluidized bed when coal was combusted with biomass (Wu et al., 2023).

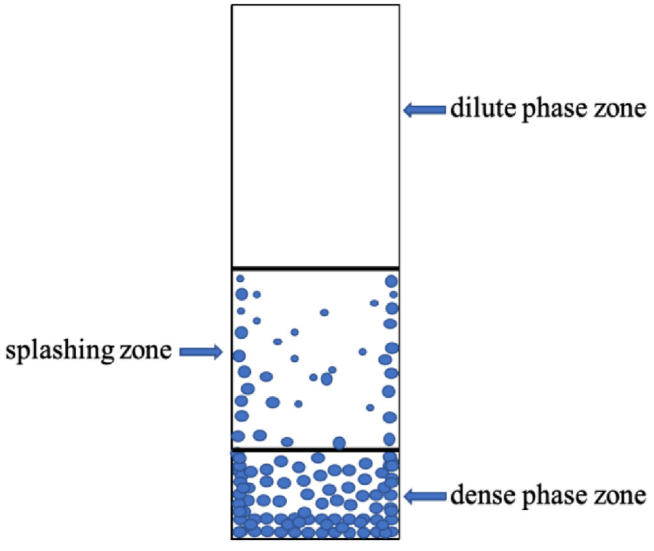

Fig. 6. The three zones are divided by particle density along the fluidized bed height.

7.2. The temperature distribution of co-firing

When coal and biomass are co-combusted in a chamber, the temperature distribution inside the chamber is critical for the heat transfer and chemical reactions between the solid and gas phases. Since the current degree of experimental analysis is typically only feasible for select points, such as the inlet, it is challenging to determine the temperature distribution throughout the whole chamber. Therefore, numerous studies have been carried out to predict the temperature distribution inside the chamber using numerical simulations. CFD modeling was used to simulate the co-firing of coal and torrefied maize straw in an industrial coal-fired boiler, and the temperature distribution was studied in the vertical combustion furnace axis. As the proportion of biomass increased from 20% to 40%, the temperature in the upper part of the furnace increased. This might be explained by the fact that the biomass was fed from the top and had a higher combustion reactivity index (C) than coal. The combustion reactivity index is defined by Eq. (7):

$$C = \frac{(\mathrm{d}m/\mathrm{d}t)_{\max}}{T_i^2} \tag{7}$$

where T_i is the ignition temperature, and $(\mathrm{d}m/\mathrm{d}t)_{\max}$ is the maximum weight loss rate. However, the temperature in the bottom of the furnace decreased, because with the increase of biomass, less coal was fed to the bottom for constant thermal power in boiler (Szufa et al., 2023). A numerical simulation found that when coal and biomass were co-combusted in a bubbling bed, the gas temperature increased with the height of the chamber due to the exothermic combustion reaction of the char and some volatiles in the fuel. However, at the location of the secondary air inlet, the gas temperature in the furnace first dropped and then rose sharply resulting from the low-temperature secondary air. In addition, with the increase in oxygen concentration, the gas temperature also rose due to the improvement of the exothermic combustion reaction (Zhou et al., 2022). To investigate the effects and suitable operating conditions for co-firing of different types of biomasses in a 300 MW coal-fired industrial boiler. A numerical simulation was conducted to study the combustion of 100% coal and the co-firing of 85% coal with 15% cotton stalks, corn straw and wheat straw, respectively. The results showed the temperature distribution along the longitudinal section of the furnace. The furnace was divided into three regions: ash hopper region, the main combustion zone and burnout area (see Fig. 7). For all the above combustion and co-firing, the temperatures of ash hopper area were the lowest, which suggested less chance of slagging. The temperatures of the main combustion zone were the highest in furnace and symmetrically distributed. Compared with the combustion of coal alone, for the co-firing of coal with corn straw, the temperature rose in the main combustion zone because the calorific value of corn straw was higher than that of low rank lignite coal. However, due to the lower calorific value of cotton stalks and wheat straw, the temperature decreased for the

Fig. 7. The regional division of a 300 MW coal-fired industrial boiler furnace.

co-firing of coal and cotton stalks and wheat straw, respectively. However, compared with the combustion of coal, the range of high temperature was broader in the main combustion region for the co-firing of coal with biomass owing to the higher content of volatiles in biomass, which contributed to the lower ignition temperature (Li et al., 2022a).

7.3. *The gas distribution of co-firing*

The co-firing of coal and biomass in the furnace involved chemical reactions between a large number of different gases. The experiments typically only measured the amount of certain gaseous pollutants in the flue gas, but the detailed distribution of gases inside the furnace remains unknown. Modeling the gas distribution by numerical simulation is a good strategy since the gas distribution profile in the furnace is crucial for figuring out where chemical reactions occur. A model simulated the co-firing of coal and biomass in a furnace using the Eulerian–Lagrangian model. With the increase in furnace height, the changing trends in the mass fraction of CO_2 were opposite to that of the O_2 mass fraction. At the bottom, as the height increased from 0 m to 2 m, a rapid decrease in the mass fraction of O_2 and the rapid increase in the mass fraction of CO_2 was observed. The main reason was that the volatile released from fuel was oxidized by O_2 to produce CO_2. The fundamental cause of the rapid increase in mass fraction of O_2 and the rapid drop in mass fraction of CO_2 as the height rose from 2 m to 6 m was the addition of secondary air. With the height continued to rise to 15 m, the rapid drop in mass fraction of O_2 and the rapid increase in CO_2 might be due to the large amount of oxygen consumption by char combustion to produce large amounts of CO_2. After a height of 15 m, the mass fractions of O_2 and CO_2 stabilized. Therefore, the lower part of a furnace (<15 m) was where the combustion reaction of coal and biomass took place. In addition, as the height of furnace increased, the mass fraction of CO first increased and then decreased. The increase in mass fraction of CO might be due to the release of the volatile from fuel. The oxidation of CO to CO_2 might be the cause of the decrease in the mass fraction of CO (Gao et al., 2023). Another model also based on Eulerian–Lagrangian frame simulated the co-firing of coal and refuse derived fuel (RDF) in a circulating fluidized bed. In the furnace of the fluidized bed, coal and RDF was fed from two dedicated feed inlets. The RDF inlet was above the coal inlet. The simulation results showed the time-averaged mass fraction of gaseous pollutants at different zones of furnace. The O_2 content was very low from the coal feed inlet to the top of the chamber. The main reason was that coal and RDF required a large amount of oxygen for co-firing, which suggested that the combustion reaction was intense in this zone. The CO content was high from the RDF feed inlet to the top of the furnace, which might be caused by incomplete combustion and pyrolysis of the fuel in this region. In this region, the NO content was low because NO could be reduced to N_2 by CO. In addition, the region contained high HCl content due to the high chloride content in RDF (Kong et al., 2020).

8. Conclusions

In general, the co-firing of coal with biomass is advantageous to reduce ignition temperature and increase ignition performance since biomass has a high level of volatility. The addition of biomass also tends to lower the generation of typical air pollutants like CO_2 and SO_x in the flue. In addition, during the growth process of biomass, due to photosynthesis, a large amount of CO_2 is absorbed from the air. Therefore, some studies suggest that biomass should be considered a carbon neutral material, or even carbon-negative, and the CO_2 released from its combustion should not be included in the CO_2 emission. If carbonaceous materials were left after combustion of biomass, the combustion of biomass would further reduce CO_2 emissions. However, due to low calorific value, the vast majority of biomasses result in lower average temperatures in the primary combustion area. In addition, because biomass ash has a low melting temperature, the co-firing is more likely to result in slagging. In order to build on the strengths and avoid the weaknesses, choosing appropriate coupling power generation technology, operational conditions (such as mixing ratios) and biomass pretreatment (such as torrefaction) are crucial. A strategy for better understanding the co-firing of coal and biomass inside the furnace is by numerical simulations.

Declaration of competing interest

The authors declare that they have no known competing financial interests or personal relationships that could have appeared to influence the work reported in this paper.

Acknowledgements

The authors appreciate the financial support from the Liao Ning Revitalization Talents Program (Grant No. XLYC2007179).

References

Abdullah, N., Safana, A. A., Sulaiman, F., & Abdullahi, I. I. (2017). A comparative analysis of physical and chemical properties of biochars and bio-oils obtained from pyrolytic process of mesocarp fibre and empty fruit bunch. *Solid State Phenomena, 268*, 387–392.

Adeleke, A. A., Odusote, J. K., Ikubanni, P. P., Olabisi, A. S., & Nzerem, P. (2022). Briquetting of subbituminous coal and torrefied biomass using bentonite as inorganic binder. *Scientific Reports, 12*, 8716.

Agbor, E., Zhang, X., & Kumar, A. (2014). A review of biomass co-firing in North America. *Renewable and Sustainable Energy Reviews, 40*, 930–943.

Ahn, S., Choi, G., & Kim, D. (2014). The effect of wood biomass blending with pulverized coal on combustion characteristics under oxy-fuel condition. *Biomass and Bioenergy, 71*, 144–154.

Akhtar, J., Sheikh, N., & Munir, S. (2017). Linear regression-based correlations for estimation of high heating values of Pakistani lignite coals. *Energy Sources, Part A: Recovery, Utilization, and Environmental Effects, 39*, 1063–1070.

Akhtar, J., Yaseen, A., & Munir, S. (2018). Effect of rice husk co-combustion with coal on gaseous emissions and combustion efficiency. *Energy Sources, Part A: Recovery, Utilization, and Environmental Effects, 40*, 1010–1018.

Asadullah, M., Adi, A. M., Suhada, N., Malek, N. H., Saringat, M. I., & Azdarpour, A. (2014). Optimization of palm kernel shell torrefaction to produce energy densified bio-coal. *Energy Conversion and Management, 88*, 1086–1093.

Barzegar, R., Yozgatligil, A., & Atimtay, A. T. (2022). *Co-combustion of high and low ash lignites with raw and torrefied biomass under air and oxy-fuel combustion atmospheres. Energy Sources, Part A: Recovery, Utilization, and Environmental Effects*. https://doi.org/10.1080/15567036.2022.2038313

Boumanchar, I., Chhiti, Y., M'hamdi Alaoui, F. E., Elkhouakhi, M., Sahibed-dine, A., Bentiss, F., Jama, C., & Bensitel, M. (2019). Investigation of (co)-combustion kinetics of biomass, coal and municipal solid wastes. *Waste Management, 97*, 10–18.

Cai, H., Liu, J., Kuo, J., Xie, W., Evrendilek, F., & Zhang, G. (2021). Ash-to-emission pollution controls on co-combustion of textile dyeing sludge and waste tea. *Science of the Total Environment, 794*, Article 148667.

Cai, P., Zhao, L. J., Wang, K., & Kong, S. T. (2014). Experiment study on mixed combustion of biomass and coal. *Advanced Materials Research, 978*, 3–6.

Chen, M., Yi, B., Li, Z., & Yuan, Q. (2020). Combustion characteristics of biomass and bituminous coal co-firing in non-isothermal and isothermal conditions. *Bioresources, 15*, 9490–9506.

China Electricity Council. (2021). *Annual development Report of China's power industry 2021*. Available at: https://www.cec.org.cn/upload/zt/fzbgzt2021/zt2021/index.html.

Demirbas, A., Dincer, K., & Topaloglu, N. (2008). Determination and calculation of combustion heats of 20 lignite samples. *Energy Sources, Part A: Recovery, Utilization, and Environmental Effects, 30*, 917–923.

Deng, L., Zhang, T., & Che, D. (2013). Effect of water washing on fuel properties, pyrolysis and combustion characteristics, and ash fusibility of biomass. *Fuel Processing Technology, 106*, 712–720.

Duan, F., Zhang, L., & Huang, Y. (2012). Dependence of bituminous coal gasification on pressure in a turbulent circulating fluidized bed. *Asia-Pacific Journal of Chemical Engineering, 7*, 822–827.

Galina, N. R., Romero Luna, C. M., Arce, G. L. A. F., & Ávila, I. (2019). Comparative study on combustion and oxy-fuel combustion environments using mixtures of coal with sugarcane bagasse and biomass sorghum bagasse by the thermogravimetric analysis. *Journal of the Energy Institute, 92*, 741–754.

Gao, R., Yin, S., Song, T., & Lu, P. (2023). Numerical simulation of co-combustion of pulverized coal and biomass in TTF precalciner. *Fuel, 334*, 126515.

Garcia, E., Mejía, M. F., & Liu, H. (2022). Fluidised bed combustion and ash fusibility behaviour of coal and spent coffee grounds blends: CO and NO_x emissions, combustion performance and agglomeration tendency. *Fuel, 326*, 125008.

Gil, M. V., Casal, D., Pevida, C., Pis, J. J., & Rubiera, F. (2010). Thermal behaviour and kinetics of coal/biomass blends during co-combustion. *Bioresource Technology, 101*, 5601–5608.

Gil, M. V., García, R., Pevida, C., & Rubiera, F. (2015). Grindability and combustion behavior of coal and torrefied biomass blends. *Bioresource Technology, 191*, 205–212.

Given, P. H., Weldon, D., & Zoeller, J. H. (1986). Calculation of calorific values of coals from ultimate analyses: Theoretical basis and geochemical implications. *Fuel, 65*, 849–854.

Gungor, A. (2013). Simulation of co-firing coal and biomass in circulating fluidized beds. *Energy Conversion and Management, 65*, 574–579.

Guo, F., He, Y., Hassanpour, A., Gardy, J., & Zhong, Z. (2020). Thermogravimetric analysis on the co-combustion of biomass pellets with lignite and bituminous coal. *Energy, 197*, 117147.

Guo, L., Zhai, M., Wang, Z., Zhang, Y., & Dong, P. (2019). Comparison of bituminous coal and lignite during combustion: Combustion performance, coking and slagging characteristics. *Journal of the Energy Institute, 92*, 802–812.

Guo, F., & Zhong, Z. (2018). Co-combustion of anthracite coal and wood pellets: Thermodynamic analysis, combustion efficiency, pollutant emissions and ash slagging. *Environmental Pollution, 239*, 21–29.

Hansen, P. F. B., Andersen, K. H., Wieck-Hansen, K., Overgaard, P., Rasmussen, I., Frandsen, F. J., Hansen, L. A., & Dam-Johansen, K. (1998). Co-Firing straw and coal in a 150-MW_e utility boiler: *In situ* measurements. *Fuel Processing Technology, 54*, 207–225.

Haykiri-Acma, H., Yaman, S., & Kucukbayrak, S. (2010). Effect of biomass on temperatures of sintering and initial deformation of lignite ash. *Fuel, 89*, 3063–3068.

Haykiri-Acma, H., Yaman, S., & Kucukbayrak, S. (2016). Combustion characteristics of torrefied biomass materials to generate power. In *Proceedings of the 2016 IEEE Smart energy Grid Engineering (SEGE)*. Oshawa, ON: Canada.

Howell, A., Beagle, E., & Belmont, E. (2018). Torrefaction of healthy and beetle kill pine and co-combustion with sub-bituminous coal. *Journal of Energy Resources Technology, 140*, Article 042002.

Huang, L., Xie, C., Liu, J., Zhang, X., Chang, K., Kuo, J., Sun, J., Xie, W., Zheng, L., Sun, S., Buyukada, M., & Evrendilek, F. (2018). Influence of catalysts on co-combustion of sewage sludge and water hyacinth blends as determined by TG-MS analysis. *Bioresource Technology, 247*, 217–225.

IEA. (2021). *Coal-fired power*. Available at: https://www.eia.gov.

IEA Bioenergy. (2022). *IEA Bioenergy annual Report 2021*. Available at: https://www.ieabioenergy.com/blog/publications/iea-bioenergy-annual-report-2021/.

Ikeda, M., Makino, H., Morinaga, H., Higashiyama, K., & Kozai, Y. (2003). Emission characteristics of NO*x* and unburned carbon in fly ash during combustion of blends of bituminous/sub-bituminous coals. *Fuel, 82*, 1851–1857.

Isaac, K., & Bada, S. O. (2020). The co-combustion performance and reaction kinetics of refuse derived fuels with South African high ash coal. *Heliyon, 6*, Article e03309.

Jenkins, B. M., Baxter, L. L., Miles, T. R., & Miles, T. R. (1998). Combustion properties of biomass. *Fuel Processing Technology, 54*, 17–46.

Jerzak, W., Kalicka, Z., Kawecka-Cebula, E., & Straka, R. (2018). Retention of S with lignite using cedarnut shell in the co-combustion process performed in a fluidized bed combustor. *Combustion Science and Technology, 190*, 707–720.

Jiang, D., Dong, C., Yang, R., Zhang, J., & Yang, Y. (2009). Modeling the gasification based biomass co-firing in a 600MW pulverized coal boiler. In *Proceedings of the 2009 International Conference on sustainable power generation and supply, Nanjing, China*.

Jiang, Y., Mori, T., Naganuma, H., & Ninomiya, Y. (2022). Effect of the optimal combination of bituminous coal with high biomass content on particulate matter (PM) emissions during co-firing. *Fuel, 316*, 123244.

Jing, N., Zhu, M., Shen, G., Wang, Q., & Zhang, D. (2016). Effect of ash preparation method on the sintering characteristics of ashes from combustion of coal and biomass blends. *Fuel, 186*, 830–837.

Jun, Z., Qian, L., Zhong, W. Q., & Yu, Z. W. (2020). Migration and transformation law of potassium in the combustion of biomass blended coal. *Journal of Fuel Chemistry and Technology, 48*, 929–936.

Junga, R., Pospolita, J., & Niemiec, P. (2020). Combustion and grindability characteristics of palm kernel shells torrefied in a pilot-scale installation. *Renewable Energy, 147*, 1239–1250.

Kai, X., Yang, T., Huang, Y., Sun, Y., He, Y., & Li, R. (2011). The effect of biomass components on the co-combustion characteristics of biomass with coal. In *Proceedings of the 2011 second International Conference on*. New York, USA: Digital Manufacturing & Automation.

Kanwal, F., Ahmed, A., Jamil, F., Rafiq, S., Uzair Ayub, H. M., Ghauri, M., Khurram, M. S., Munir, S., Inayat, A., Abu Bakar, M. S., Moogi, S., Lam, S., & Park, Y. (2021). Co-combustion of blends of coal and underutilised biomass residues for environmental friendly electrical energy production. *Sustainability, 13*, 4881.

Kim, D. W., Lee, J. M., Kim, J. S., & Kim, J. J. (2007). Co-combustion of Korean anthracite with bituminous coal in two circulating fluidized bed combustors. *Korean Journal of Chemical Engineering, 24*, 461–465.

Kong, D., Wang, S., Zhou, M., Luo, K., Hu, C., Li, D., & Fan, J. (2020). Three-dimensional full-loop numerical simulation of co-combustion of coal and refuse derived fuel in a pilot-scale circulating fluidized bed boiler. *Chemical Engineering Science, 220*, 115612.

Kopczyński, M., Lasek, J. A., Iluk, A., & Zuwała, J. (2017). The co-combustion of hard coal with raw and torrefied biomasses (willow (Salix viminalis), olive oil residue and waste wood from furniture manufacturing). *Energy, 140*, 1316–1325.

Krzywański, J., Rajczyk, R., & Nowak, W. (2014). Model research of gas emissions from lignite and biomass co-combustion in a large scale CFB boiler. *Chemical and Process Engineering, 35*, 217–231.

Liang, W., Jiang, C., Wang, G., Ning, X., Zhang, J., Guo, X., Xu, R., Wang, P., Ye, L., Li, J., & Wang, C. (2022). Research on the co-combustion characteristics and kinetics of agricultural waste hydrochar and anthracite. *Renewable Energy, 194*, 1119–1130.

Li, F., Li, Y., Fan, H., Wang, T., Guo, M., & Fang, Y. (2019). Investigation on fusion characteristics of deposition from biomass vibrating grate furnace combustion and its modification. *Energy, 174*, 724–734.

Li, F., Yu, B., Zhao, W., Wang, J., Xu, M., Fan, H., … Fang, Y. (2022b). Investigation on formation mechanisms of ash and deposit from cotton stalk vibrating grate boiler combustion based on their characteristics. *Fuel, 323*, 124446.

Li, F., Zhao, W., Fan, H., Xu, M., Lu, J., Zhao, C., Guo, M., Guo, Q., & Fang, Y. (2021). Effects of sludge on the ash fusion behaviors of corn stalk and its modification mechanisms. *Fuel, 293*, 120378.

Li, J., Wang, Z., & Ma, C. (2022a). Numerical simulation and combustion analysis of coal and biomass co-combustion. *MATEC Web of Conferences, 355*, Article 02013.

Li, S., Li, H., Li, W., Xu, M., Eddings, E. G., Ren, Q., & Lu, Q. (2017). Coal combustion emission and ash formation characteristics at high oxygen concentration in a 1 MW_{th} pilot-scale oxy-fuel circulating fluidized bed. *Applied Energy, 197*, 203–211.

Li, Y., Zhou, H., Li, N., Tao, C., Liu, Z., & Cen, K. (2018). Experimental study of the combustion and NO emission behaviors during cofiring coal and biomass in O_2/N_2 and O_2/H_2O. *Asia-Pacific Journal of Chemical Engineering, 13*, Article e2198.

Li, Y. G., Wang, Y. Z., Zhu, W. B., & Sun, Y. (2020). Study on the effect of Si-Al components in pulverized coal ash on corrosion in heating surface of biomass boiler. *Key Engineering Materials, 837*, 89–94.

Lin, Y. L., & Zheng, N. Y. (2021). Biowaste-to-biochar through microwave-assisted wet co-torrefaction of blending mango seed and passion shell with optoelectronic sludge. *Energy, 225*, 120213.

Lin, Y. L., Zheng, N. Y., & Hsu, C. H. (2021a). Torrefaction of fruit peel waste to produce environmentally friendly biofuel. *Journal of Cleaner Production, 284*, 124676.

Lin, Y. L., Zheng, N. Y., & Lin, C. S. (2021b). Repurposing *Washingtonia filifera* petiole and *Sterculia foetida* follicle waste biomass for renewable energy through torrefaction. *Energy, 223*, 120101.

Lin, Y. L., Zheng, N. Y., & Wang, H. C. (2022). Sludge dewatering through H_2O_2 lysis and ultrasonication and recycle for energy by torrefaction to achieve zero waste: An environmental and economical friendly technology. *Renewable and Sustainable Energy Reviews, 155*, 111857.

Liu, H., Han, K., Liu, M., Niu, S., & Lu, C. (2015b). A thermogravimetric analysis of co-combustion characteristics of biomass and coal in an O_2/CO_2Atmosphere. *Energy Sources, Part A: Recovery, Utilization, and Environmental Effects, 37*, 2451–2457.

Liu, H., Wang, Y., Hu, H., Fu, B., Yao, H., & Wendt, J. O. L. (2020b). Enrichment mechanism of arsenic in fine ash deposits during co-combustion of rice husk and coal. *Fuel, 281*, Article 118712.

Liu, J., Wang, S., Wang, J., Hou, F., Duan, C., Zhang, X., Zhao, Z., Cui, F., Liu, K., Wang, H., Hu, Z., & Yang, X. (2021). Application of sludge coupling power generation technology in coal-fired power plant. In *IOP Conference Series: Earth and environmental Science* (Vol. 632), Article 042024.

Liu, J. H., Li, B., Qiu, X. L., Yang, H. R., & Liu, Q. (2012). Co-Combustion of biomass with bituminous coal in A CFB boiler. In *Proceedings of the Asia-Pacific power and energy Engineering Conference (APPEEC), Shanghai, China*.

Liu, L., Ren, S., Yang, J., Jiang, D., Guo, J., Pu, Y., & Meng, X. (2022b). Experimental study on K migration, ash fouling/slagging behaviors and CO_2 emission during co-combustion of rice straw and coal gangue. *Energy, 251*, Article 123950.

Liu, Q., Zhong, W., Gu, J., & Yu, A. (2020a). Three-dimensional simulation of the co-firing of coal and biomass in an oxy-fuel fluidized bed. *Powder Technology, 373*, 522–534.

Liu, Q., Zhong, W., Yu, A., & Wang, C. H. (2022a). Modelling the co-firing of coal and biomass in a 10 kW_{th} oxy-fuel fluidized bed. *Powder Technology, 395*, 43–59.

Liu, X., Chen, M., & Wei, Y. (2015a). Kinetics based on two-stage scheme for co-combustion of herbaceous biomass and bituminous coal. *Fuel, 143*, 577–585.

Liu, X., Chen, M., & Wei, Y. (2016b). Assessment on oxygen enriched air co-combustion performance of biomass/bituminous coal. *Renewable Energy, 92*, 428–436.

Liu, X., Yang, X., Xie, G., & Yu, Y. (2021). NO emission characteristic during fluidized combustion of biomass with limestone addition. *Fuel, 291*, Article 120264.

Liu, X., Wu, X., & Wang, J. (2018). Substantial upgrading of a high-ash lignite by hydrothermal treatment followed by $Ca(OH)_2$ digestion/acid leaching. *Fuel, 222*, 269–277.

Liu, Z., Saydaliev, H. B., Lan, J., Ali, S., & Anser, M. K. (2022b). Assessing the effectiveness of biomass energy in mitigating CO_2 emissions: Evidence from Top-10 biomass energy consumer countries. *Renewable Energy, 191*, 842–851.

Liu, Z., Hu, W., Jiang, Z., Mi, B., & Fei, B. (2016a). Investigating combustion behaviors of bamboo, torrefied bamboo, coal and their respective blends by thermogravimetric analysis. *Renewable Energy, 87*, 346–352.

Lu, G., Zhang, K., & Cheng, F. (2018). The fusion characteristics of ashes from anthracite and biomass blends. *Journal of the Energy Institute, 91*, 797–804.

Lv, Y., Xu, L., Niu, Y., Wang, G., Lei, Y., Huang, H., & Hui, S. E. (2022). Investigation on ash deposition formation during co-firing of coal with wheat straw. *Journal of the Energy Institute, 100*, 148–159.

Ma, L., Goldfarb, J. L., Song, J., Chang, C., & Ma, Q. (2022). Enhancing cleaner biomass-coal co-combustion by pretreatment of wheat straw via washing versus hydrothermal carbonization. *Journal of Cleaner Production, 366*, 132991.

Mazumder, S., Saha, P., & Reza, M. T. (2022). Co-hydrothermal carbonization of coal waste and food waste: Fuel characteristics. *Biomass Conversion and Biorefinery, 12*, 3–13.

Mehmood, S., Reddy, B. V., & Rosen, M. A. (2012). Energy analysis of a biomass co-firing based pulverized coal power generation system. *Sustainability, 4*, 462–490.

Mikulčić, H., Cerinski, D., Baleta, J., & Wang, X. (2019). Improving pulverized coal and biomass co-combustion in a cement rotary kiln by computational fluid dynamics. *Chemical Engineering & Technology, 42*, 2539–2545.

Mostafa, M. E., Khedr, Y. M., Ling, P., Chi, H., Hu, S., Wang, Y., Su, S., Elsayed, S. A., & Xiang, J. (2021). Experimental and numerical modelling of solid and hollow biomass pellets high-temperature rapid oxy-steam combustion: The effect of integrated CO_2/H_2O concentration. *Fuel, 303*, 121249.

Mu, L., Li, T., Wang, Z., Chen, B., Shang, Y., & Yin, H. (2022). Slag formation characteristics of co-combustion of bituminous coal with algae and woody biomass. *Renesable Energy Resources, 40*(2), 143–151 (in Chinese).

Munir, S., Daood, S. S., Nimmo, W., Cunliffe, A. M., & Gibbs, B. M. (2009). Thermal analysis and devolatilization kinetics of cotton stalk, sugar cane bagasse and shea meal under nitrogen and air atmospheres. *Bioresource Technology, 100*, 1413–1418.

Namkung, H., Lee, Y. J., Park, J. H., Song, G. S., Choi, J. W., Choi, Y. C., Park, S. J., & Kim, J. G. (2018). Blending effect of sewage sludge and woody biomass into coal on combustion and ash agglomeration behavior. *Fuel, 225*, 266–276.

National Bureau of Statistics. (2021). *China statistical yearbook-2021*. Beijing, China: China Statistics Press.

National Energy Administration. (2018). *The first pilot coal-fired coupling technical transformation completed 72-hour trial operation*. Available at: http://www.nea.gov.cn/2018-07/18/c_137333016.htm.

Ni, Z., Bi, H., Jiang, C., Sun, H., Zhou, W., Qiu, Z., He, L., & Lin, Q. (2022). Influence of biomass on coal slime combustion characteristics based on TG-FTIR, principal component analysis, and artificial neural network. *Science of the Total Environment, 843*, Article 156983.

Nowak, K., & Rabczak, S. (2021). Co-combustion of biomass with coal in grate water boilers at low load boiler operation. *Energies, 14*, 2520.

Otero, M., Gómez, X., García, A. I., & Morán, A. (2007). Effects of sewage sludge blending on the coal combustion: A thermogravimetric assessment. *Chemosphere, 69*, 1740–1750.

Patil, A., Dhote, L., Middey, A., Pandey, R. A., & Kumar, S. (2022). Emission characteristics for combustion of sludge with coal in a grate furnace aimed at boiler application. *Fuel, 324*, Article 124598.

Pérez, A., Ruiz, B., Fuente, E., Calvo, L. F., & Paniagua, S. (2021). Pyrolysis technology for *Cortaderia selloana* invasive species. Prospects in the biomass energy sector. *Renewable Energy, 169*, 178–190.

Priyanto, D. E., Matsunaga, Y., Ueno, S., Kasai, H., Tanoue, T., Mae, K., & Fukushima, H. (2017). Co-firing high ratio of woody biomass with coal in a 150-MW class pulverized coal boiler: Properties of the initial deposits and their effect on tube corrosion. *Fuel, 208*, 714–721.

Priyanto, D. E., Wada, C., Sato, N., Ueno, S., & Mae, K. (2018). Fly ash transformation and fouling tendency during co-firing biomass with coal. *Journal of the Japan Institute of Energy, 97*, 216–221.

Riaza, J., Gil, M. V., Álvarez, L., Pevida, C., Pis, J. J., & Rubiera, F. (2012). Oxy-fuel combustion of coal and biomass blends. *Energy, 41*, 429–435.

Sahu, S., Sarkar, P., Mukherjee, A., Adak, A., & Chakraborty, N. (2013). Studies on the co-combustion behaviour of coal/biomass blends using thermogravimetric analysis. *International Journal of Emerging Technology and Advanced Engineering, 3*, 131–138.

Sakthivel, C., Gopal, P., Rameshkumar, C., & Kumar, B. S. (2018). Co-combustion analysis of lignite coal and groundnut shell using TGA. *Journal of Applied Fluid Mechanics, 11*, 7578.

Saleem, M. (2022). Possibility of utilizing agriculture biomass as a renewable and sustainable future energy source. *Heliyon, 8*, Article e08905.

Selvakumaran, P., & Bakthavatsalam, A. K. (2015). Effect of chemical composition of ash on sintering of lignites in circulating fluid bed combustion and successful operation of large CFBC boilers. *Applied Thermal Engineering, 85*, 135–147.

Shi, K., Oladejo, J. M., Yan, J., & Wu, T. (2019). Investigation on the interactions among lignocellulosic constituents and minerals of biomass and their influences on co-firing. *Energy, 179*, 129–137.

Soka, O., & Oyekola, O. (2020). A feasibility assessment of the production of char using the slow pyrolysis process. *Heliyon, 6*, Article e04346.

Spiegl, N., Long, X., Berrueco, C., Paterson, N., & Millan, M. (2021). Oxy-fuel co-gasification of coal and biomass for negative CO_2 emissions. *Fuel, 306*, 121671.

Standardization Administration. (2009). *Chinese classification of coals*. Beijing, China: Standards Press of China.

Stephan, A., Wolf, C., Fendt, S., & Spliethoff, H. (2017). Online corrosion measurements in small- and mid-scale during pulverised biomass/coal co-combustion. *Energy Procedia, 120*, 309–316.

Szufa, S., Piersa, P., Junga, R., Błaszczuk, A., Modliński, N., Sobek, S., Marczak-Grzesik, M., Adrian, Ł., & Dzikuć, M. (2023). Numerical modeling of the co-firing process of an *in situ* steam-torrefied biomass with coal in a 230 MW industrial-scale boiler. *Energy, 263*, 125918.

Tao, G., Lestander, T. A., Geladi, P., & Xiong, S. (2012). Biomass properties in association with plant species and assortments I: A synthesis based on literature data of energy properties. *Renewable and Sustainable Energy Reviews, 16*, 3481–3506.

Toptas, A., Yildirim, Y., Duman, G., & Yanik, J. (2015). Combustion behavior of different kinds of torrefied biomass and their blends with lignite. *Bioresource Technology, 177*, 328–336.

Torres, R., Valdez, B., Beleño, M. T., Coronado, M. A., Stoytcheva, M., García, C., … Montero, G. (2021a). Char production with high-energy value and standardized properties from two types of biomass. *Biomass Conversion and Biorefinery, 13*, 4831–4847.

Uguz, O., Haykiri-Acma, H., & Yaman, S. (2020). Burning resistance of lignitic coals under oxygen-enriched conditions. *Journal of Energy Resources Technology, 142*, Article 082301.

Umar, D. F., Monika, I., & Handoko, S. (2021). TG-DSC investigation of co-combustion characteristics of blends sawdust and coal. *IOP Conference Series: Earth and Environmental Science, 749*, Article 012016.

United Nations. (2016). *The Paris Agreement*. Available at: https://www.un.org/tr/node/104330.

Vamvuka, D., & Sfakiotakis, S. (2011). Combustion behaviour of biomass fuels and their blends with lignite. *Thermochimica Acta, 526*, 192–199.

Wang, C., Zhou, L., Fan, G., Yuan, M., Zhao, L., Tang, G., … Che, D. (2021a). Experimental study on ash morphology, fusibility, and mineral transformation during co-combustion of antibiotic filter residue and biomass. *Energy, 217*, Article 119345.

Wang, C., Zhao, L., Sun, R., Hu, Y., Tang, G., Chen, W., Du, Y., & Che, D. (2019). Effects of silicon-aluminum additives on ash mineralogy, morphology, and transformation of sodium, calcium, and iron during oxy-fuel combustion of Zhundong high-alkali coal. *International Journal of Greenhouse Gas Control, 91*, 102832.

Wang, C. B., Wang, J. X., & Lei, M. (2013). Low-temperature ignition characteristics of coal/biomass blends. *Journal of Chinese Society of Power Engineering, 33*(3), 218–223.

Wang, G., Zhang, J., Shao, J., Liu, Z., Zhang, G., Xu, T., Guo, J., Wang, H., Xu, R., & Lin, H. (2016). *Thermal behavior and kinetic analysis of co-combustion of waste biomass/low rank coal*.

Wang, G., Zhang, J., Shao, J., & Ren, S. (2014). Characterisation and model fitting kinetic analysis of coal/biomass co-combustion. *Thermochimica Acta, 591*, 68–74.
Wang, H., Zheng, Z. M., Yang, L., Liu, X. L., Guo, S., & Wu, S. H. (2015). Experimental investigation on ash deposition of a bituminous coal during oxy-fuel combustion in a bench-scale fluidized bed. *Fuel Processing Technology, 132*, 24–30.
Wang, H., Guo, S., Yang, L., Wei, X., Zhang, S., & Wu, S. (2017). Impacts of water vapor and AAEMs on limestone desulfurization during coal combustion in a bench-scale fluidized-bed combustor. *Fuel Processing Technology, 155*, 134–143.
Wang, Q., Han, K., Wang, P., Li, S., & Zhang, M. (2020). Influence of additive on ash and combustion characteristics during biomass combustion under O_2/CO_2 atmosphere. *Energy, 195*, Article 116987.
Wang, Y., Zou, L., Shao, H., Bai, Y., Liu, Y., Zhao, Q., & Li, F. (2022). Co-combustion of high alkali coal with municipal sludge: Thermal behaviour, kinetic analysis, and micro characteristic. *Science of the Total Environment, 838*, Article 156489.
Wang, Y. K., Deng, L., Jia, Z. P., Dan, H. J., Wei, X., Tan, Z. Q., & Wang, Z. C. (2021b). Influence of large-scale direct coupled biomass power generation on coal-fired units. *Thermal Power Generation, 50*(12), 80–91.
Wen, S., Zou, H., Liu, H., Huang, J., Evrendilek, D. E., Yan, Y., Li, W., & Liu, J. (2021). Combustion behaviors of complex incense stick residues: Multivariate Gaussian process-based optimization of thermal, kinetic, thermodynamic, emission, and ash responses. *Fuel, 293*, Article 120439.
Wu, J., Wang, Y., Han, J., Li, X., Yu, D., Xu, M., & Wendt, J. O. (2019). Ash formation and deposition in oxy-fuel combustion of rice husk, coal, and their blend with 70% inlet O_2. *Energy & Fuels, 34*, 890–899.
Wu, W., Duan, L., Duan, Y., Li, L., Liu, D., & Pallarès, D. (2023). Three-dimensional full-loop numerical simulation of coal and sludge co-combustion in a circulating fluidized bed. *Fuel, 337*, Article 127235.
Wolf, C., Stephan, A., Fendt, S., & Spliethoff, H. T. (2017). Measuring gaseous HCl emissions during pulverised co-combustion of high shares of straw in an entrained flow reactor. In *Proceedings of the 11th European Conference on industrial furnaces and boilers (INFUB), Algarve, Portugal*.
Xie, L., Lv, Y., & Xu, L. (2021). The influence of the high potassium biomass on the ash fusion characteristics of coal. *Journal of the Energy Institute, 95*, 52–60.
Xue, Z., Zhong, Z., & Lai, X. (2020). Investigation on gaseous pollutants emissions during co-combustion of coal and wheat straw in a fluidized bed combustor. *Chemosphere, 240*, Article 124853.
Xu, Y., Yang, K., Zhou, J., & Zhao, G. (2020). Coal-biomass co-firing power generation technology: Current status, challenges and policy implications. *Sustainability, 12*, 3692.
Xu, J., Yu, D., Fan, B., Zeng, X., Lv, W., & Chen, J. (2014). Characterization of ash particles from co-combustion with a Zhundong coal for understanding ash deposition behavior. *Energy & Fuels, 28*, 678–684.
Yang, L. C., Pang, Q. H., He, Z. J., Zhang, J. H., Zhan, W. L., & Lü, N. (2021a). Kinetic study on co-combustion of pulverized anthracite and bituminite for blast furnace injection. *Journal of Iron and Steel Research International, 28*, 949–964.
Yang, W., Pudasainee, D., Gupta, R., Li, W., Wang, B., & Sun, L. (2022). Particulate matter emission during MSW/RDF/WW combustion: Inorganic minerals distribution, transformation and agglomeration. *Fuel Processing Technology, 228*, Article 107166.
Yan, P., Xiao, C., Xu, L., Yu, G., Li, A., Piao, S., & He, N. (2020). Biomass energy in China's terrestrial ecosystems: Insights into the nation's sustainable energy supply. *Renewable and Sustainable Energy Reviews, 127*, Article 109857.
Yang, X., Luo, Z., Liu, X., Yu, C., Li, Y. A., & Ma, Y. (2021b). Experimental and numerical investigation of the combustion characteristics and NO emission behaviour during the co-combustion of biomass and coal. *Fuel, 287*, Article 119383.
Yao, X., Zhou, H., Xu, K., Chen, S., Ge, J., & Xu, Q. (2020a). Systematic study on ash transformation behaviour and thermal kinetic characteristics during co-firing of biomass with high ratios of bituminous coal. *Renewable Energy, 147*, 1453–1468.
Yao, X., Zhou, H., Xu, K., Xu, Q., & Li, L. (2020b). Investigation on the fusion characterization and melting kinetics of ashes from co-firing of anthracite and pine sawdust. *Renewable Energy, 145*, 835–846.
Yin, K., Zhou, Y. M., Yao, Q. Z., Fang, C., & Zhang, Z. W. (2012). Thermogravimetric analysis of the catalytic effect of metallic compounds on the combustion behaviors of coals. *Reaction Kinetics, Mechanisms and Catalysis, 106*, 369–377.
Yu, D., & Chen, M. (2016). Oxygen enriched co-combustion of biomass and bituminous coal. *Energy Sources, Part A: Recovery, Utilization, and Environmental Effects, 38*, 994–1001.
Yu, D., Morris, W. J., Erickson, R., Wendt, J. O. L., Fry, A., & Senior, C. L. (2011). Ash and deposit formation from oxy-coal combustion in a 100 kW test furnace. *International Journal of Greenhouse Gas Control, 5*, S159–S167.
Zhakupov, D., Kulmukanova, L., Sarbassov, Y., & Shah, D. (2022). Flue gas analysis for biomass and coal co-firing in fluidized bed: Process simulation and validation. *International Journal of Coal Science & Technology, 9*, 59.
Zhang, X., Li, K., Zhang, C., & Wang, A. (2020). Performance analysis of biomass gasification coupled with a coal-fired boiler system at various loads. *Waste Management, 105*, 84–91.
Zhang, B., & Lu, G. W. (2013). Experimental study on combustion characteristics of biomass and coal blended. *Advanced Materials Research, 805–806*, 200–207.
Zhang, Y. X., Luo, H. L., & Wang, C. (2021). Progress and trends of global carbon neutrality pledges. *Climate Change Research, 17*(1), 88–97.
Zhang, Z., & Zeng, Q. (2019). Numerical simulation and experimental analysis on nitrogen and sulfur oxides emissions during the co-combustion of Longyan anthracite and sawmill sludge. *Fuel, 254*, Article 115611.
Zhao, Y., Wang, S., Shen, Y., & Lu, X. (2013). Effects of nano-TiO_2 on combustion and desulfurization. *Energy, 56*, 25–30.
Zheng, N. Y., Lee, M., Lin, Y. L., & Samannan, B. (2020). Microwave-assisted wet co-torrefaction of food sludge and lignocellulose biowaste for biochar production and nutrient recovery. *Process Safety and Environmental Protection, 144*, 273–283.
Zhou, A., Xu, H., Xu, M., Yu, W., Li, Z., & Yang, W. (2020b). Numerical investigation of biomass co-combustion with methane for NO_x reduction. *Energy, 194*, Article 116868.
Zhou, J., Liu, Q., Zhong, W. Q., & Yu, Z. W. (2020a). Migration and transformation law of potassium in the combustion of biomass blended coal. *Journal of Fuel Chemistry and Technology, 48*, 929–936.
Zhou, M., Wang, S., Luo, K., & Fan, J. (2022). Three-dimensional modeling study of the oxy-fuel co-firing of coal and biomass in a bubbling fluidized bed. *Energy, 247*, Article 123496.
Zhuang, X., Song, Y., Zhan, H., Yin, X., & Wu, C. (2019). Synergistic effects on the co-combustion of medicinal biowastes with coals of different ranks. *Renewable Energy, 140*, 380–389.